Multidimensional microclimate velocities alter the picture of shifting climates in tropical forests

Lydia G. Soifer[1,2], James Ball[1], Hamish Asmath[3], Ilya M.D. Maclean[4] & David Coomes[1*]

[1] Department of Plant Sciences, University of Cambridge, UK

[2] School of Natural Resources and Environment, University of Florida, USA

[3] Department of Geography, University of the West Indies, St. Augustine, Trinidad and Tobago

[4] Environment and Sustainability Institute, University of Exeter, UK

* Corresponding author email: dac18@cam.ac.uk

1. ABSTRACT

Climate velocity—the speed and direction species must move to track climate change—is often estimated without accounting for vegetation-driven microclimatic variation. Using airborne lidar data from a tropical montane rainforest, we generated high-resolution 3D maps of topography and canopy structure to mechanistically model near-ground and within-canopy microclimates. Microclimate-derived temperature velocities were slower, revealing reduced dispersal demands. For terrestrial species, fine-scale maximum temperature velocities were frequently oriented toward dense vegetation patches in addition to higher elevations, contrasting traditional macroclimate-based predictions. Arboreal organisms could further reduce velocities by moving vertically within the canopy to cooler microhabitats, highlighting the role of 3D habitat structure in mitigating exposure. These results demonstrate that vegetation complexity creates localized microrefugia, enabling species persistence under warming by altering both the magnitude and direction of required range shifts. Our findings emphasize the need to integrate fine-scale habitat heterogeneity into climate resilience strategies to more accurately forecast biodiversity responses.

Climate change is causing the redistribution of species globally, with range shifts generally occurring toward higher latitudes and elevations[1–3]. Climate velocity indicates how quickly and in which direction suitable climatic conditions for species are shifting locally[4,5] and estimates the distance per year a species occurring at any given location would have to move to keep pace with climate change[4,5]. However, range shifts often lag behind rates of climate velocity or occur in directions opposing dominant climate gradients, suggesting species are unable to migrate fast enough to keep pace with the effects of global warming[2,6–8].

Local climate velocity is calculated as the temporal rate of climate change divided by the spatial rate of climate change, with climate variables typically extracted from global databases of free-air conditions at relatively coarse spatial scales[4,5,9]. However, these data overlook the role of climatic buffering by forest canopies, which may reduce velocities and alter their direction by providing local refugia that allow species to persist in increasingly inhospitable landscapes[10–13]. A better understanding of local climate velocities that account for microclimate variability is therefore urgently needed to provide insight into the impacts of climate change on range shifts[14,15].

Forests are three-dimensional ecosystems where complex vegetative structures produce microclimatic variability, both horizontally along the forest floor and vertically within the canopy[12,16,17]. By reducing solar radiation and airflow, vegetation reduces temperature extremes, which can produce highly heterogeneous microclimates beneath structurally complex canopies that influence the distribution of terrestrial and arboreal species[12,17–19]. As the climate warms, species may move along microclimate gradients produced by vegetation to maintain their thermal niche[20,21]. Building upon previous research addressing macroclimate velocities[4,5,22,23], we model microclimates to examine how vegetation impacts the speed and direction of microclimate velocities along forest floors and within the three-dimensional structure of forest canopies at three spatial grains, as climate

change may impact species at the scale of a few centimeters or hundreds of meters, depending on organism size[24,25].

Tropical forests are threatened by novel high temperatures, which are contributing to species' redistribution[26,27]. Our study focused on tropical montane forests in northern Trinidad, where an airborne lidar scan allowed us to generate a digital elevation model (DEM), canopy height model (CHM), and map of the vertical distribution of plant area density across 1300 km^2 of the mountain range, spanning 900 m in elevation (Supplementary fig. **Error! Reference source not found.**). We integrate these maps with ERA5 macroclimate data in a mechanistic microclimate model to predict maximum temperature of the warmest month and minimum temperature of the coldest month across the land surface and within the canopy at 20 m, 100 m, and 1 km resolutions within forests for 1960 and 2015 (Fig. **1**; Supplementary figs. **2, 3**). We then calculate microclimate velocities across spatial scales over the land surface and advance microclimate research by extending the climate velocity algorithm to three-dimensions within the canopy. These velocities represent the distance and direction that a ground-dwelling or arboreal species at any given location would need to move locally to track warming temperatures (see methods).

2. LOCAL VARIATION IN FOREST STRUCTURE REDUCES CLIMATE VELOCITY

In montane ecosystems, including in the tropics, species are lagging behind rates of climate change[6,28]. By decoupling microclimate from macroclimate conditions and/or increasing spatial microclimate heterogeneity, vegetation could reduce microclimate velocities. To examine impacts of vegetation on climate velocities, we compared the average temporal rate of climate change, spatial rate of climate change, and climate velocity calculated based on free-air and microclimate conditions at 1 km and 100 m spatial resolutions (see methods).

Accounting for impacts of vegetation on microclimates reduced climate velocities for maximum temperatures across spatial scales (Fig. **2**; Extended data table **1**; Extended data fig. **1**). These reductions could have arisen from decreases in the temporal rate or increases in the spatial rate of climate change, recalling that climate velocity is calculated as the temporal rate divided by the spatial rate. We found that changes in temporal rates were not responsible, as they were similar to, or exceeded, free-air warming rates (Fig. **2**, Supplementary fig. **4**). Given that understories are experiencing novel temperatures across the tropics[26], it is unsurprising that the temporal rate does not substantially contribute to climate velocity declines.

Instead, strong increases in the spatial rate of climate change generated by local variation in canopy structure and therefore buffering capacity were responsible for reducing microclimate velocities[29,30] (Fig. **2**; Supplementary fig. **5**). Across the land surface, maximum temperature velocities were 1.6-times slower than free-air velocities at a 1 km resolution and 2 times slower than free-air velocities at a 100 m resolution (Fig. **2**; Extended data table **1**). Over 55 years, these reduced velocities shorten the distance that maximum temperature isotherms shift from 4.2 km to 2.7 km at a 1 km resolution and from 1.1 km to 540 m at a 100 m resolution. Differences were greater between free-air and 3D microclimate velocities due to the additional vertical microclimatic heterogeneity. Relative to free-air velocities, 3D microclimate velocities were 161.3-times slower at a 1 km resolution and 52-times slower at a 100 m resolution. These declines translated into shifts of only 15 m and 11 m over 55 years. Similar patterns were observed for minimum temperatures (Fig. **2**; Extended data fig. **2**). Increases in the spatial rate of climate change reduced land-surface and within-canopy velocities relative to free-air velocities across spatial resolutions, though the temporal rate of microclimate change was also slower than free-air conditions (Extended data table **1**; Supplementary figs. **6, 7**).

Slower microclimate velocities suggest that species' ranges may not have to shift as quickly as previously thought to keep pace with rates of climate change, because high microclimate heterogeneity produced by variation in vegetation density shortens the distance organisms must move to reach cooler climates. Examining range shifts in the context of free-air velocities may therefore overestimate climatic lags in redistribution. Overestimation may be particularly prevalent in tropical lowland forests, where low free-air temperature variation produces high climate velocities[5]. Accounting for variation in vegetation structure and understory microclimate may improve our understanding of species' redistribution patterns in these regions.

3. GRANULARITY OF CLIMATE ESTIMATES

Within forests, species respond to climatic conditions at a variety of spatial scales from centimeters to kilometers depending on the size of the organism[25,31]. We examine the impact of spatial grain on microclimate velocities by comparing velocities calculated at 1 km, 100 m, and 20 m resolutions.

Maximum temperature velocities mirrored patterns previously observed for macroclimate velocities, increasing at coarser spatial grains due to the inverse relationship between spatial grain and climatic heterogeneity[9,23,31]. At fine spatial grains, the capacity to detect variation in the structural complexity of vegetation increases microclimate heterogeneity[12]. Microclimate velocities at a 20 m resolution across the land surface were therefore low, at a median rate of only 3.4 m/yr. At coarser spatial grains, microclimate variability declined as pixels were averaged over space, while the temporal rate of climate change was less affected (Fig. **3**). Lower spatial rates of climate change therefore increased microclimate velocities to median rates of 9.8 m/yr at a 100 m resolution and 48.4 m/yr at a 1 km resolution. However, the impact of spatial grain largely disappeared in three-dimensions, with over 99% of within-canopy velocities under 1 m/yr, due to high microclimatic

heterogeneity imposed by the vertical thermal gradient (Fig. **3**; Extended Data Table **1**). Minimum temperature velocities exhibited a similar pattern (Fig. **3**; Extended Data Table **1**).

The rate at which species are expected to move thus depends on the spatial grain at which they perceive microclimate. Species that respond to microclimate at larger spatial grains will need to shift ranges more quickly to keep pace with climate change, because fine-grained microclimate heterogeneity may not provide thermal refuge. In contrast, species responding to climate conditions at finer spatial scales or in three-dimensions may be able to move shorter distances to remain in suitable climate conditions. For example, heavily shaded understory environments, as well as structural microhabitats, including tree holes and leaf litter, provide cool microclimates that reduce exposure to extreme temperatures[32,33]. These slower velocities at fine spatial grains may represent opportunities for thermoregulatory behavior rather than range shifts to reduce exposure to temperature extremes within thermally variable local environments[21].

4. LOCAL VARIATION IN FOREST STRUCTURE ALTERS THE DIRECTION OF CLIMATE VELOCITY

Traditional views of species range shifts assume movement toward higher latitudes and elevations as species track their preferred thermal niche[14]. However empirical evidence challenges this notion[2,7,8]. For example, a recent study by Rubenstein et al.[8] found that only 47% of documented range shifts align with these expectations, which may be attributed to numerous factors, including persistence in local microclimates[12] or range shifts along thermal gradients that oppose latitudinal or elevational gradients[13]. To explore the impact of vegetation on the direction of climate velocity, we examined whether climate velocities were directed upslope or toward areas with denser vegetation using circular correlations[34,35] between the angle of climate velocity in the latitude-longitude plane and the angle a species would need to move to reach higher elevations or denser vegetation. We then graphed the

152 distribution of differences between the angle of climate velocity and the direction of higher
153 elevation or denser vegetation to visualize these correlations (Fig. **4**).

154 The direction of free-air velocities for maximum and minimum temperatures at 1 km
155 and 100 m spatial resolutions were directed upslope, exhibiting strong positive correlations
156 with the direction needed to reach higher elevations and not with the direction needed to reach
157 denser vegetation (Figs. **4**; Extended Data Table **1**). Small differences between the direction of
158 free-air climate velocities and the direction of higher elevations support the pervasive view
159 that species will shift upslope in the tropics[36].

160 At the same spatial resolutions, land surface velocities for maximum temperatures
161 exhibited positive correlations with both the direction of higher elevation and the direction of
162 denser vegetation (Figs. **4**; Extended Data Table **1**). Reducing the spatial resolution to 20 m
163 produced greater variability in velocity directions, but maintained positive correlations with
164 denser vegetation, while exhibiting negative correlations with the direction of higher
165 elevation. Dense vegetation may therefore reverse the direction of range shifts by altering
166 local climate gradients.

167 When dispersal capacity, biotic interactions, or life history traits prevent upslope range
168 shifts at a pace matching that of climate change[1,6,7], species may find refuge from increasing
169 maximum temperatures by moving to locally denser forest patches. Forest density is a strong
170 predictor of microclimatic decoupling, reducing diurnal temperature ranges and increasing
171 maximum temperature offsets relative to more sparsely vegetated areas[19,37]. These
172 vegetatively dense microclimatic refugia may function similarly to topoclimate refugia, which
173 are found in convergent environments, such as valley bottoms, and have provided thermal
174 refuge to species during past periods of climatic instability[22]. Maintaining dense forest patches
175 within structurally diverse environments may therefore slow range contraction and extirpation
176 of heat-intolerant species and reduce thermophilization of understory communities[38].

However, movement to denser vegetation may not protect populations at warm range edges, which may already be restricted to the coolest microhabitats in the local landscape[13]. These populations are unable to respond to slow microclimate velocities directed toward dense vegetation and must instead shift upslope to reach cooler environments. Furthermore, populations at warm range edges that are increasingly restricted to denser forest patches may face density declines as the extent of suitable habitat shrinks. Therefore, while dense forest patches may increase short-term persistence in the landscape, populations may face extirpation as the geographic extent of locally suitable microclimates shrink with increasing temperatures. Species responding to fine scale climate gradients will thus depend on the conservation and restoration of forests with complex vegetative structure where taller and denser patches offset maximum temperatures that may otherwise exceed the narrow critical thermal limits of tropical understory species[39,40].

Land surface velocities for minimum temperatures were also directed upslope at a 100 m resolution, but in contrast to maximum temperatures, exhibited negative correlations with the direction of denser vegetation at 100 m and 20 m resolutions (Extended Data Table **1**), because understory thermal minima are generally warmer than macroclimate conditions[41,42]. Minimum temperatures have strong impacts on species distribution limits at cold range edges, particularly at higher latitudes[43]. While potentially having a lower impact on range dynamics than maximum temperatures in the tropics, the direction of minimum temperature velocities may therefore be especially applicable to expansion dynamics at cold range edges in temperate and boreal forests, and reflect local reductions in minimum temperature constraints that could broaden microhabitat use for peripheral populations.

5. 3D VELOCITIES DEMONSTRATE ADDITIONAL REFUGIA FOR ARBOREAL SPECIES

In response to climate change, species may move across multi-dimensional climate gradients[20]. In addition to elevational gradients, arboreal species can move across vertical thermal gradients, which can exhibit temperature increases from the ground to the canopy up to 1.6 times the change in temperature across 200 m in elevation[44]. To examine how the spatial dimensionality of climate influences velocities, we calculated the direction of 3D temperature velocities, which represent directions in which arboreal species would need to move to keep pace with climate change. Rather than being directed toward higher elevations or denser vegetation (Fig. **4**), over 88% of maximum temperature velocities across spatial scales were directed vertically downward. However, downward shifts in temperature isotherms were not ubiquitous for either maximum or minimum temperatures. Maximum temperature velocities directed vertically upward occurred more frequently in areas with sparser vegetation (Extended Data Fig. **3**), where vertical temperature gradients are reversed, such that the understory is warmer than the canopy[16] (Extended Data Fig. **4**). Furthermore, only 52.4%, 66.9%, and 77.8% of minimum temperature velocity vectors exhibited downward movement at 20 m, 100 m, and 1 km spatial scales, respectively, due to weaker vertical gradients in minimum temperatures (Extended Data Fig. **4**).

For tropical arboreal species whose ranges will be most impacted by increasing maximum temperatures, slow downward-directed velocities indicate opportunities for organisms to dwell further down forest canopies without the need to migrate over the land surface. Indeed, vertical shifts in habitat use have been documented across short spatial and temporal gradients for arboreal frogs, which shift toward the ground at lower elevations and during the dry season[44,45]. Whether these thermoregulatory behaviors persist over longer time spans in response to warming climates remains unknown.

Yet, the full 3D forest environment is not available to all species. Resource distributions, including food and light, limit vertical habitat availability for arboreal plants and animals. For example, low light in the lower canopy may prevent colonization by epiphytes, and predator-prey, mutualistic, and competitive interactions may prevent vertical reorganization of animal communities despite changing climates[46]. Furthermore, arboreal species have evolved mobility traits, such as flying and gliding locomotion and adhesive toe pads[46], which may compromise their success in lower canopy or terrestrial environments where vegetation structure differs. If species are unable to extend their vertical habitat use, ranges could become vertically compressed into narrower canopy strata[47]. After reaching the lower limit of suitable vertical habitat, arboreal species would be expected to move in the speed and direction of 2D velocities within the canopy, which exceed velocities across the land surface (Supplementary methods; Supplementary table **1**; Supplementary Fig. **8**). Although georeferenced occurrence records for numerous taxa are now readily accessible through platforms such as GBIF[48], these records rarely contain information regarding height above the ground. Combining our models with empirical data on shifts in vertical habitat use will be critical to evaluate the extent to which species follow 3D climate velocities.

6. TOWARD A GENERAL UNDERSTANDING OF MICROCLIMATE VELOCITY

Overall, we found that accounting for impacts of vegetation on climate variability reduces velocities and alters their direction. Notably, microclimate velocities revealed an additional dimension to isotherm shifts determined by the density of vegetation and height above ground. In addition to shifting across elevations, maximum temperature velocities were often directed toward denser vegetation or toward the ground, while minimum temperature velocities were often directed toward sparser vegetation at fine spatial resolutions. Species may therefore reduce exposure to warming maximum temperatures by increasing their use of, or becoming restricted to, understory habitats beneath dense vegetation, reflecting the multi-

249 dimensionality of range shift dynamics that are increasingly recognized as critical for
250 understanding species' redistribution in a changing climate[20].
251 While our study is restricted to temperature velocities within a tropical montane
252 system, the mechanistic nature of the microclimate model and climate velocity calculations
253 allows our conclusions to be generalized to other biomes, such as temperate and boreal forests
254 where minimum temperatures strongly impact cold range limits[43]. Our approach could also be
255 used to evaluate the velocity of microclimate variables associated with water stress, such as
256 vapor pressure deficit. At macroclimate scales, diverging precipitation and temperature
257 velocity may prevent species from maintaining their historical climatic niche and cause
258 reshuffling of ecological communities[9,49]. However, at microclimatic scales, the forest
259 understory is both cooler and more humid than macroclimate conditions[16,17,19]. Moving under
260 dense vegetation to seek refuge from high maximum temperatures would therefore
261 simultaneously reduce hydric stress, preventing substantial mismatches between the direction
262 of microclimate velocity vectors representing thermal and hydric conditions.
263 The capacity to escape high temperatures by exploiting thermally complex landscapes
264 will be critical for species with limited dispersal capacity and species living in landscapes
265 with homogeneous macroclimate gradients, such as lowland tropical rainforests[5,36]. However,
266 predicted increases in thermal offsets that provide refuge are contingent upon forests
267 maintaining constant buffering capacity[42]. Deforestation combined with tree mortality due to
268 increasing disturbances from droughts, wildfires, and insect outbreaks are reducing canopy
269 cover globally[50,51], yet our models assume constant vegetation cover due to lack of repeat lidar
270 surveys. Vegetation declines could increase land surface and within-canopy climate velocities
271 by increasing rates of microclimate warming[52] and homogenizing microclimate variability.
272 Forest understory communities would thus be expected to exhibit faster rates of change
273 relative to predictions made assuming constant vegetation structure[53]. Maintaining and

restoring structurally complex forests will therefore be critical to reduce microclimate velocities and provide microclimatic refugia beneath dense vegetation that offer alternative routes to prolonging maintenance of climatic niches under global warming.

7. ONLINE METHODS

All analyses took place in the Northern Range of Trinidad, a Caribbean Island that lies off the coast of Venezuela, due to the availability of a wall-to-wall lidar survey of the island.

7.1. Climate grids

We mechanistically modeled maximum temperature of the warmest month and minimum temperature of the coldest month for 1960 and 2015, as climate extremes have a greater impact on species recruitment and survival than climate means[54–56]. The microclimate models were initially produced at a 20 m resolution using the R package 'microclimf'[57,58], which uses the physical laws of thermodynamics to connect macroclimate data to local microclimate conditions based on the impacts of topography and vegetation on solar radiation and windspeed, and allows approximation of microclimate conditions in regions of the world lacking in-situ microclimate sensor networks[59]. We chose the years 1960 and 2015 because they best represent average temperature during the decades 1951-1960 and 2011-2020, and a 20 m resolution based on a sensitivity analysis to determine a cell size that captured fine-scale variation in vegetation structure while minimizing outliers (Supplementary Methods). These models were produced at 2 m above the ground for land-surface climate estimates, and then from 5 m to 40 m above the ground at 5 m intervals (i.e. 2 m, 5 m, 10 m, etc.) to estimate within-canopy conditions (see supplementary methods for detailed description). We then coarsened these microclimate models to 100 m and 1 km resolutions by aggregating and averaging grid cells. Regardless of spatial resolution, we refer to these as microclimate models, as they represent climate conditions experienced by terrestrial or arboreal organisms.

298 We obtained free-air temperatures at a 100 m spatial resolution, by mechanistically
299 modelling climate conditions, accounting for impacts of topography, but not vegetation, using
300 the R package 'microclima'[60]. We obtained free-air climate conditions at an ~ 1 km resolution
301 from CHELSA version 2.1[61,62] to represent a readily accessible and frequently used
302 macroclimate data source. Because CHELSA data were not available for 1960, we estimated
303 the 1960 climate based on offsets between CHELSA and ERA5 data in 1980. We do not
304 model free-air conditions at a finer resolution because the processes mediating the relationship
305 between topography and climate act at scales from hundreds of meters to kilometers[63].
306 However, in doing so, we may miss identifying localized thermal extremes in extremely
307 heterogeneous terrain[64].
308 The climate models are based on first principles of energy conservation[57]. They first
309 apply a topographic correction for adiabatic lapse rate and then estimate microclimate
310 parameters by solving the Penmen-Monteith equation assuming the relationships between
311 sensible heat fluxes and latent heat fluxes remain in balance. Microclimf has been validated
312 against over 400 in situ temperature loggers spanning four continents in different land cover
313 types, including 70 loggers in tropical rainforests, yielding more accurate predictions than
314 other global climate models (e.g., Worldclim and ERA5)[26,65].
315 Model inputs included spatially gridded data describing macroclimate, topography,
316 vegetation structure and characteristics, soil type, and habitat type. Gridded climate data were
317 obtained from ERA5[66] using the 'mcera5' R package[67] at an ~25 km resolution and at hourly
318 time intervals for 1960 and 2015. Topography and vegetation layers were derived from
319 discrete return Light Detection and Ranging (LiDAR) data, which was collected in June 2014.
320 The consultant provided classifications for last return ground points and non-ground points,
321 which were then kriged in ArcMap 10.5 to develop a digital elevation model (DEM) of
322 ground points and a digital surface model (DSM) of non-ground points at a 1 m resolution. A

canopy height model was developed by subtracting the DEM from the first-return non-ground points. The height of each point above the ground was computed in LASTools using the 'lasheight' function[68]. The DEM and canopy height model were then aggregated and averaged to a 20 m resolution. Plant area index (PAI; m2/m2) and plant area density (PAD; m2/m3) were calculated at a 20 m horizontal resolution and 1 m vertical resolution based on the Beer-Lambert law for light transmittance through a turbid medium and assuming an extinction coefficient of 0.5[69]. We estimated PAI and PAD seasonality by modeling monthly fluctuations in MODIS LAI with a generalized additive mixed model and applying a standard offset across all months based on the difference in MODIS LAI and LiDAR PAI (see supplementary methods for further details).

We mapped soil type according to the USDA soil classification triangle with sand, silt, and clay content obtained from the SoilGrids database at a 250 m resolution[70,71]. We obtained habitat type data from a classification of Trinidadian vegetation[72] and reclassified habitat types to those specified in the 'microclimf' R package to estimate other vegetation parameters, including the ratio of vertical to horizontal leaf foliage, maximum stomatal conductance, leaf reflectance, canopy clumsiness, and leaf diameter[57] (Supplementary Material).

To model microclimates in the Northern Range from remotely sensed data, we had to make assumptions that compromised model accuracy. First, the lack of repeat lidar surveys required that we assume constant vegetation over time. We also assume that soil and vegetation properties are constant within broad categories and concur with average parameters identified by the model. Furthermore, we note that our models are limited to a small area relative to the global tropics. This is due to computing limitations, as our models at a 20 m resolution include over 2 million climate velocity estimates across the land surface and over 4.5 million estimates in three dimensions within the canopy spanning the Northern mountain

348 range of Trinidad for both maximum and minimum temperatures. However, the mechanistic
349 nature of the climate models and climate velocity calculations allows our conclusions to be
350 generalized to other regions.

351 **7.2. Climate Velocity**

352 Climate velocity is calculated as the temporal rate of climate change divided by the
353 spatial rate of climate change[4,5]

$$\frac{\Delta x}{\Delta t} = \frac{\Delta C/\Delta t}{\Delta C/\Delta x} \qquad \text{(Equation 1)}$$

354 where x is distance, C is the climate variable of interest, and t is time. We calculated
355 two-dimensional (land surface) and three-dimensional (within-canopy) microclimate
356 velocities for maximum temperature of the warmest month (°C) and minimum temperature of
357 the coldest month (°C) at three spatial scales — 1 km, 100 m, and 20 m resolutions. The
358 vertical resolution of all 3D velocities was 5 m. We restrict 3D microclimate velocities to the
359 upper half of the forest as measured from the ground to the canopy, because species
360 occupying the lower canopy can only move a few meters downwards in response to warming.
361 We compared 100 m and 1 km microclimate velocities to two-dimensional free-air velocities
362 at a 100 m resolution (calculated from free-air climate models) and at an ~1 km resolution
363 (calculated from CHELSA climate data).

364 Climate velocity calculations were conducted in the R programming language[73]
365 adapting code from García Molinos et al.[74] (Supplementary methods). We calculated the
366 temporal rate of climate change as the slope of temperature change between 1960 and 2015.
367 The spatial rate of climate change represents the average temperature change in °C/m between
368 neighboring grid cells. For each grid cell, the spatial rate in 2D is defined based on a 3 x 3
369 grid around the central cell. For each pair of adjacent cells, the temperature differences are
370 calculated and divided by the distance between cell centers. Differences between cells that
371 neighbor each other to the west and east were averaged to produce the x dimension of the

spatial gradient, and differences between cells that neighbor each other to the north and south were averaged to produce the y dimension of the spatial gradient. When calculating averages, differences that did not include the focal cell were weighted by $1/\sqrt{2}$. The 2D spatial rate for each grid cell, *i*, is then calculated as $spatialrate_i = \sqrt{x_i^2 + y_i^2}$, where x_i represents the east-west dimension of the spatial gradient for grid cell *i*, and y_i represents the north-south dimentsion of the spatial gradient for grid cell *i* (Supplementary methods).

To calculate the 3D spatial rate of climate change, we took a similar approach, but made calculations based on adjacent voxels in a 3 x 3 x 3 cube (i.e., the central voxel and the 6 voxels that share a surface with the central one in the cube). We similarly calculated mean temperature differences in the x and y dimensions, but additionally calculated the differences between the central voxel and the voxel below it and the central voxel and the voxel above it. Vertical differences were divided by the height of each voxel (5 m) to obtain the °C/m that temperature changes vertically. These vertical differences were averaged to produce the z dimension of the spatial rate of climate change. The 3D spatial rate of climate change for each voxel, *i*, is then calculated as $spatialrate_i = \sqrt{x_i^2 + y_i^2 + z_i^2}$. For 2D and 3D calculations at a 20 m resolution, we applied an elevational correction to account for the increase in distance that must be traveled if moving parallel to a slope (Supplementary methods).

To calculate climate velocity (m/yr), we took the absolute value of the temporal rate of climate change divided by the spatial rate of climate change. For 3D velocities, we only considered vectors that fell within the canopy, which we defined as falling between 50% and 100% of the relative height of the forest (where relative height is calculated as height of the climate velocity vector divided by canopy height). Additionally, we excluded velocities occurring in non-forested grid cells, as identified by a habitat classification for Trinidad[72], as well as those that exceeded the 99th quantile. These high values occur when the spatial rate of

climate change is extremely small and do not accurately represent projected range shifts, particularly when temporal rates of climate change are relatively small.

The direction of climate velocity is the direction of the 2D or 3D vector describing the spatial rate of climate change. We calculated the direction of climate velocity in the latitude/longitude plane as the angle from north (i.e., 0° = north, 180° = south). For 3D velocities, we additionally calculated the vertical angle of movement from horizontal (where horizontal is parallel to the ground). The vertical angle ranges from -90° to 90°, where -90° indicates that the velocity vector is pointed directly toward the ground with no horizontal movement, and 90° indicates the velocity vector is pointed directly upward with no horizontal movement.

To determine whether climate velocities were directed upslope, we calculated the angular difference between the direction opposite to the aspect and the direction of climate velocity. To determine whether climate velocities were directed toward denser vegetation, we calculated the average direction of denser vegetation using the same method that we used to calculate the spatial rate of climate velocity. We then took the angular difference between the average direction of denser vegetation and the direction of climate velocity. We plotted angular differences using proportional histograms to show the proportion of grid cells where climate velocity is directed toward higher elevations or denser vegetation. An angular difference of 0° indicates climate velocities are directed upslope or toward denser vegetation and a difference of 180° indicates that climate velocities are directed downslope or toward sparser vegetation. Finally, we calculated the circular correlation between the direction of climate velocity and the direction of higher elevation or denser vegetation[34,35].

8. FIGURES

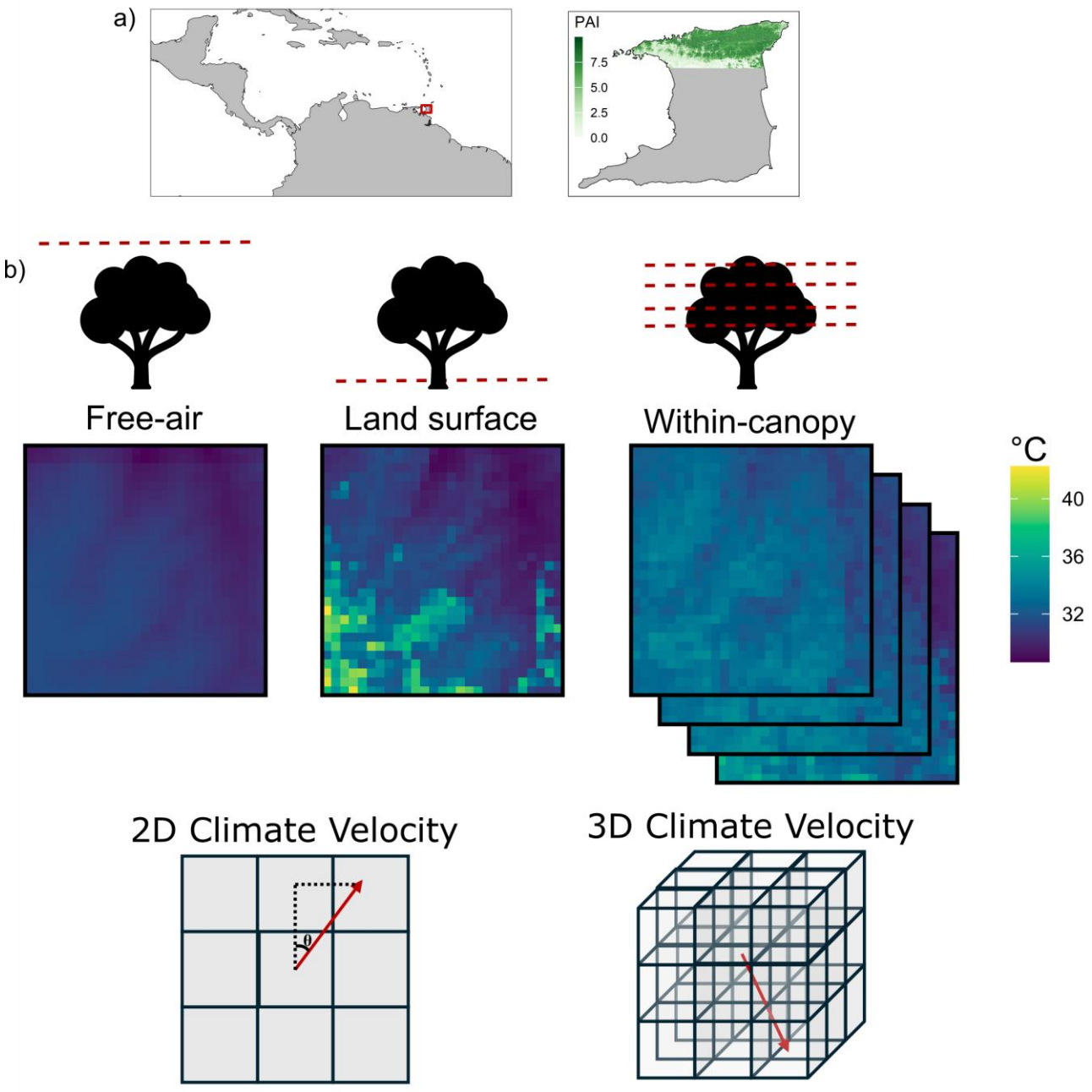

Figure 1: a) Plant area index in the northern mountain range of Trinidad. b) Three representations of climate and climate velocity at a 100 m resolution. Free-air climates at 100 m were mechanistically modelled and represent conditions accounting for impacts of topography but not vegetation. Land surface microclimates represent conditions 2 m above the ground and were mechanistically modelled accounting for impacts of topography and vegetation. 3D within canopy microclimates were modelled at 5 m intervals from the ground

to the top of the canopy. Climate velocity is represented by the red arrows. The length of the arrow represents the speed of climate velocity. For 2D climate velocities, which were calculated using free-air and land surface climate maps, the angle of the arrow from north (θ) represents the direction of climate velocity. For 3D microclimate velocities calculated from within-canopy climate maps, the angle of the arrow from north represents the horizontal direction of velocity and the angle of the arrow from horizontal represents the vertical direction of velocity.

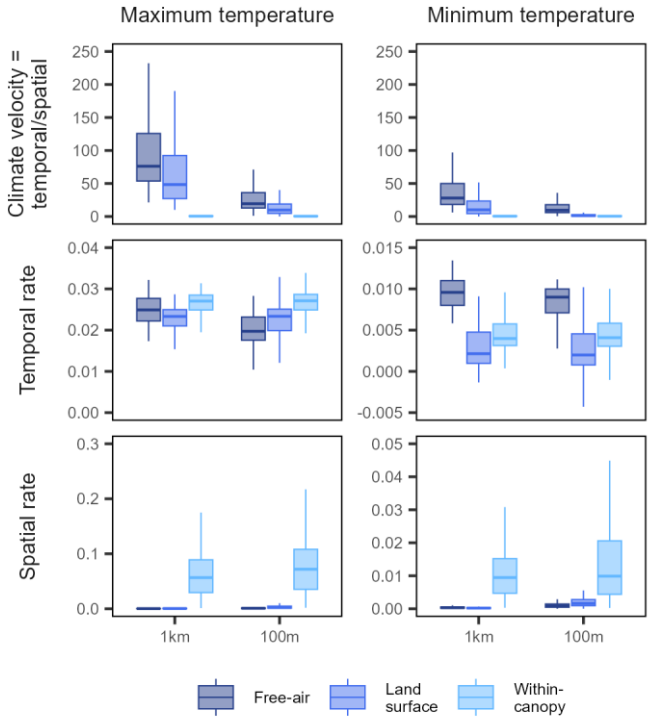

Figure 2: Climate velocity (m/yr), the temporal rate of climate change (°C/yr), and the spatial rate of climate change (°C/m) in the Northern Range of Trinidad calculated for free-air, land surface, and within-canopy climate conditions at 1 km and 100 m spatial resolutions. Free-air and land-surface velocities are calculated in two dimensions and within-canopy velocities are calculated in three-dimensions. Boxplots display median and 25th and 75th percentiles, with upper and lower whiskers corresponding to 1.5 times the IQR from the 25th or 75th percentiles. Note that y-axes differ between maximum and minimum temperatures.

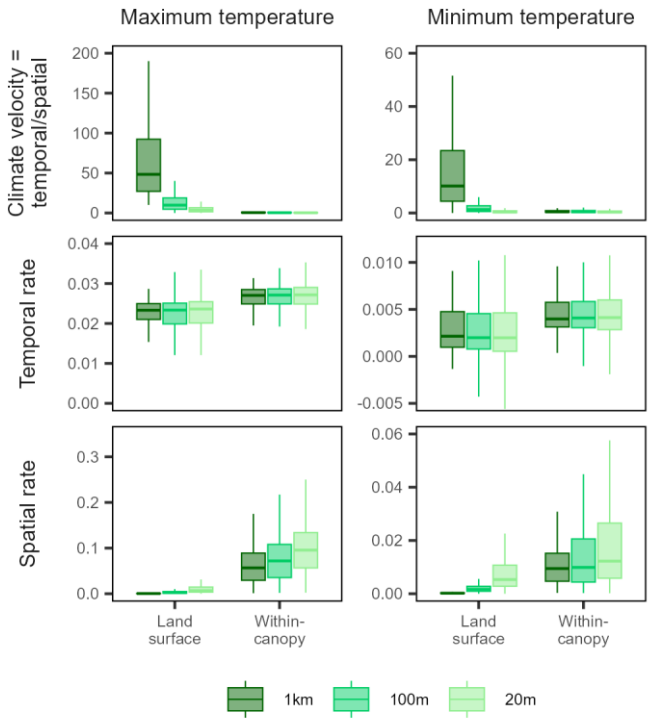

Figure 3: Microclimate velocity (m/yr), the temporal rate of climate change (°C/yr), and the spatial rate of climate change (°C/m) in the Northern Range of Trinidad calculated at 1 km, 100 m, and 20 m spatial resolutions within the forest. Land-surface velocities are calculated in two dimensions at 2 m above the ground and within-canopy velocities are calculated in three-dimensions at 5 m vertical intervals within the upper half of the canopy. Boxplots display median and 25th and 75th percentiles, with upper and lower whiskers corresponding to 1.5 times the IQR from the 25th or 75th percentiles. Note that y-axes differ between maximum and minimum temperatures.

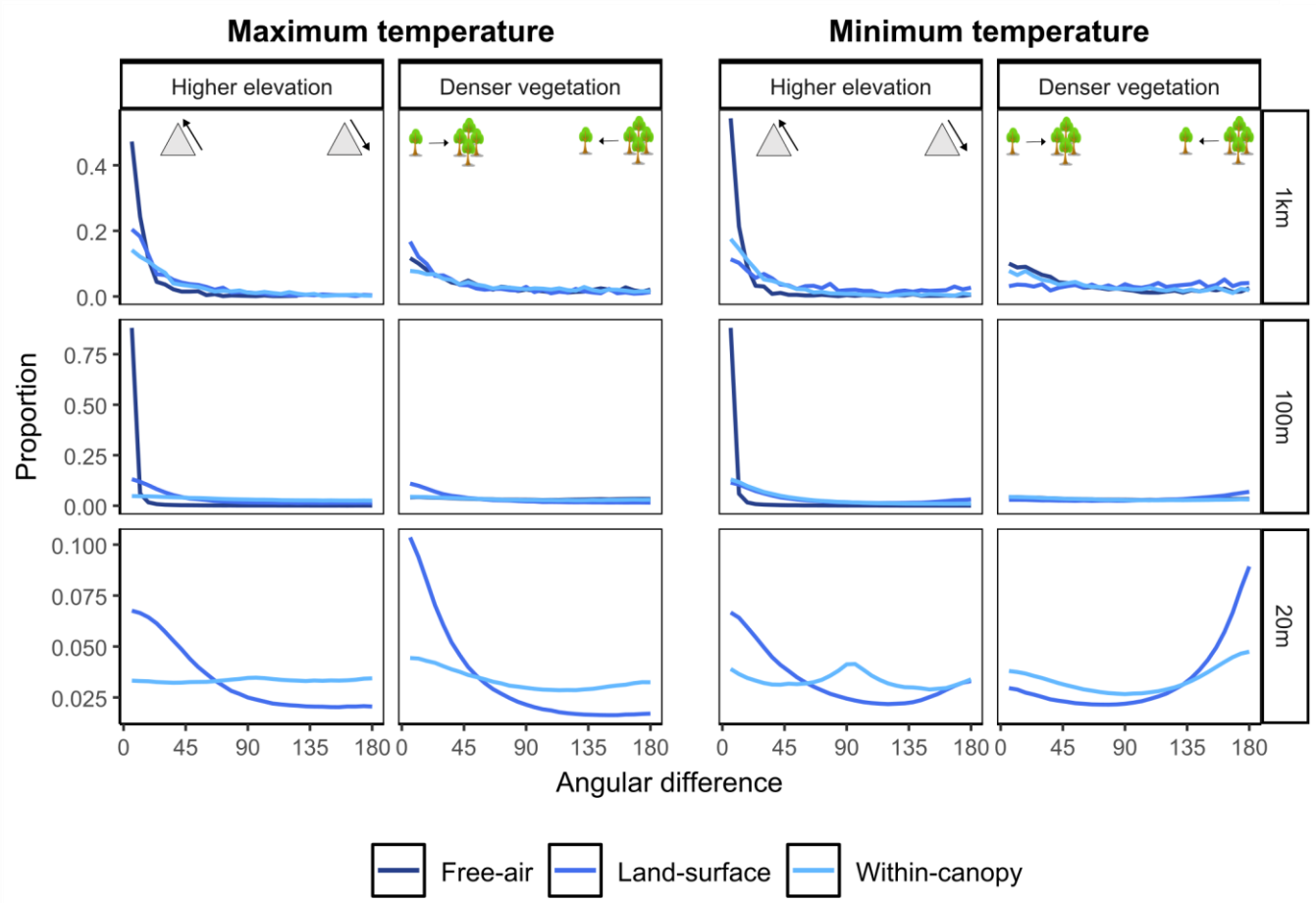

Figure 4: The proportion of grid cells with climate velocity directed toward a higher elevation or toward denser vegetation. The x-axis represents the angular difference between the direction of maximum or minimum temperature velocity and the direction a species would need to move to reach a higher elevation or denser vegetation. An angular difference of zero indicates that the direction of climate velocity is pointed toward a higher elevation (i.e., upslope) or toward denser vegetation. An angular difference of 180 indicates that the direction of climate velocity is pointed downslope or away from denser vegetation. The y-axis represents the proportion of grid cells exhibiting a given angular difference. Proportions were calculated based on 15-degree intervals. Land surface velocities are 2 m above the ground and within-canopy velocities are 3D velocities in the top half of the forest structure measured from the ground to the canopy.

9. REFERENCES

1. Chen, I.-C., Hill, J. K., Ohlemüller, R., Roy, D. B. & Thomas, C. D. Rapid range shifts of species associated with high levels of climate warming. *Science* **333**, 1024–1026 (2011).
2. Lawlor, J. A. *et al.* Mechanisms, detection and impacts of species redistributions under climate change. *Nat Rev Earth Environ* **5**, 351–368 (2024).
3. Parmesan, C. & Yohe, G. A globally coherent fingerprint of climate change impacts across natural systems. *Nature* **421**, 37–42 (2003).
4. Burrows, M. T. *et al.* The pace of shifting climate in marine and terrestrial ecosystems. *Science* **334**, 652–655 (2011).
5. Loarie, S. R. *et al.* The velocity of climate change. *Nature* **462**, 1052–1055 (2009).
6. Feeley, K. J. *et al.* Upslope migration of Andean trees. *Journal of Biogeography* **38**, 783–791 (2011).
7. Lenoir, J. *et al.* Species better track climate warming in the oceans than on land. *Nat Ecol Evol* **4**, 1044–1059 (2020).
8. Rubenstein, M. A. *et al.* Climate change and the global redistribution of biodiversity: Substantial variation in empirical support for expected range shifts. *Environmental Evidence* **12**, 7 (2023).
9. Dobrowski, S. Z. *et al.* The climate velocity of the contiguous United States during the 20th century. *Global Change Biology* **19**, 241–251 (2013).
10. Haesen, S. *et al.* Microclimate reveals the true thermal niche of forest plant species. *Ecology Letters* **26**, 2043–2055 (2023).
11. Lembrechts, J. J., Nijs, I. & Lenoir, J. Incorporating microclimate into species distribution models. *Ecography* **42**, 1267–1279 (2019).

12. Lenoir, J., Hattab, T. & Pierre, G. Climatic microrefugia under anthropogenic climate change: Implications for species redistribution. *Ecography* **40**, 253–266 (2017).
13. Maclean, I. M. D. & Early, R. Macroclimate data overestimate range shifts of plants in response to climate change. *Nat. Clim. Chang.* **13**, 484–490 (2023).
14. Lenoir, J. & Svenning, J.-C. Climate-related range shifts – a global multidimensional synthesis and new research directions. *Ecography* **38**, 15–28 (2015).
15. Brito-Morales, I. *et al.* Climate velocity can inform conservation in a warming world. *Trends in Ecology & Evolution* **33**, 441–457 (2018).
16. Vinod, N. *et al.* Thermal sensitivity across forest vertical profiles: Patterns, mechanisms, and ecological implications. *New Phytologist* **237**, 22–47 (2023).
17. De Frenne, P. *et al.* Forest microclimates and climate change: Importance, drivers and future research agenda. *Glob Change Biol* **27**, 2279–2297 (2021).
18. Hardwick, S. R. *et al.* The relationship between leaf area index and microclimate in tropical forest and oil palm plantation: Forest disturbance drives changes in microclimate. *Agricultural and Forest Meteorology* **201**, 187–195 (2015).
19. Jucker, T. *et al.* Canopy structure and topography jointly constrain the microclimate of human-modified tropical landscapes. *Glob Change Biol* **24**, 5243–5258 (2018).
20. Fredston, A. L. *et al.* Reimagining species on the move across space and time. *Trends in Ecology & Evolution* **0**, (2025).
21. Pinsky, M. L., Comte, L. & Sax, D. F. Unifying climate change biology across realms and taxa. *Trends in Ecology & Evolution* **37**, 672–682 (2022).
22. Dobrowski, S. Z. A climatic basis for microrefugia: The influence of terrain on climate. *Global Change Biology* **17**, 1022–1035 (2011).
23. Heikkinen, R. K. *et al.* Fine-grained climate velocities reveal vulnerability of protected areas to climate change. *Sci Rep* **10**, 1678 (2020).

24. Pincebourde, S. & Woods, H. A. There is plenty of room at the bottom: Microclimates drive insect vulnerability to climate change. *Current Opinion in Insect Science* **41**, 63–70 (2020).

25. Potter, K. A., Woods, A. H. & Pincebourde, S. Microclimatic challenges in global change biology. *Glob Change Biol* **19**, 2932–2939 (2013).

26. Trew, B. T. *et al.* Novel temperatures are already widespread beneath the world's tropical forest canopies. *Nat. Clim. Chang.* **14**, 753–759 (2024).

27. Fadrique, B. *et al.* Widespread but heterogeneous responses of Andean forests to climate change. *Nature* **564**, 207–212 (2018).

28. Chan, W.-P. *et al.* Climate velocities and species tracking in global mountain regions. *Nature* 1–7 (2024) doi:10.1038/s41586-024-07264-9.

29. Ismaeel, A. *et al.* Patterns of tropical forest understory temperatures. *Nat Commun* **15**, 549 (2024).

30. Menge, J. H., Magdon, P., Wöllauer, S. & Ehbrecht, M. Impacts of forest management on stand and landscape-level microclimate heterogeneity of European beech forests. *Landsc Ecol* **38**, 903–917 (2023).

31. Wiens, J. A. Spatial Scaling in Ecology. *Functional Ecology* **3**, 385–397 (1989).

32. Pottier, J. *et al.* The accuracy of plant assemblage prediction from species distribution models varies along environmental gradients. *Global Ecology and Biogeography* **22**, 52–63 (2013).

33. Scheffers, B. R., Edwards, D. P., Diesmos, A., Williams, S. E. & Evans, T. A. Microhabitats reduce animal's exposure to climate extremes. *Global Change Biology* **20**, 495–503 (2014).

34. Jammalamadaka, S. & Sarma, Y. A correlation coefficient for angular variables. *Statistical Theory and Data Analysis* **2**, 349–364 (1988).

35. Tsagris, M. *et al.* Directional: A collection of functions for directional data analysis. R package version 7.0. (2024).
36. Colwell, R. K. & Feeley, K. J. Still little evidence of poleward range shifts in the tropics, but lowland biotic attrition may be underway. *Biotropica* **57**, e13358 (2025).
37. Blonder, B. *et al.* Extreme and Highly Heterogeneous Microclimates in Selectively Logged Tropical Forests. *Front. For. Glob. Change* **1**, 5 (2018).
38. Borderieux, J., Gégout, J.-C. & Serra-Diaz, J. M. Extinction drives recent thermophilization but does not trigger homogenization in forest understorey. *Nat Ecol Evol* **8**, 695-704 (2024).
39. Tewksbury, J. J., Huey, R. B. & Deutsch, C. A. Putting the Heat on Tropical Animals. *Science* **320**, 1296–1297 (2008).
40. Sunday, J. M. *et al.* Thermal-safety margins and the necessity of thermoregulatory behavior across latitude and elevation. *Proceedings of the National Academy of Sciences* **111**, 5610–5615 (2014).
41. De Frenne, P. *et al.* Global buffering of temperatures under forest canopies. *Nat Ecol Evol* **3**, 744–749 (2019).
42. De Lombaerde, E. *et al.* Maintaining forest cover to enhance temperature buffering under future climate change. *Science of The Total Environment* **810**, 151338 (2022).
43. Normand, S. *et al.* Importance of abiotic stress as a range-limit determinant for European plants: Insights from species responses to climatic gradients. *Global Ecology and Biogeography* **18**, 437–449 (2009).
44. Scheffers, B. R. *et al.* Increasing arboreality with altitude: A novel biogeographic dimension. *Proc. R. Soc. B.* **280**, 20131581 (2013).
45. Basham, E. W. & Scheffers, B. R. Vertical stratification collapses under seasonal shifts in climate. *Journal of Biogeography* **47**, 1888–1898 (2020).

46. Xing, S. *et al.* Ecological patterns and processes in the vertical dimension of terrestrial ecosystems. *Journal of Animal Ecology* **92**, 538–551 (2023).
47. Jorda, G. *et al.* Ocean warming compresses the three-dimensional habitat of marine life. *Nat Ecol Evol* **4**, 109–114 (2020).
48. GBIF: The Global Biodiversity Information Facility. What is GBIF? https://www.gbif.org/what-is-gbif (2025).
49. Ordonez, A. & Williams, J. W. Projected climate reshuffling based on multivariate climate-availability, climate-analog, and climate-velocity analyses: Implications for community disaggregation. *Climatic Change* **119**, 659–675 (2013).
50. Curtis, P. G., Slay, C. M., Harris, N. L., Tyukavina, A. & Hansen, M. C. Classifying drivers of global forest loss. *Science* **361**, 1108–1111 (2018).
51. Hartmann, H. *et al.* Climate Change Risks to Global Forest Health: Emergence of Unexpected Events of Elevated Tree Mortality Worldwide. *Annual Review of Plant Biology* **73**, 673–702 (2022).
52. Zellweger, F. *et al.* Forest microclimate dynamics drive plant responses to warming. *Science* **368**, 772–775 (2020).
53. De Frenne, P. *et al.* Microclimate moderates plant responses to macroclimate warming. *Proceedings of the National Academy of Sciences* **110**, 18561–18565 (2013).
54. Inouye, D. w. The ecological and evolutionary significance of frost in the context of climate change. *Ecology Letters* **3**, 457–463 (2000).
55. Murali, G., Iwamura, T., Meiri, S. & Roll, U. Future temperature extremes threaten land vertebrates. *Nature* **615**, 461–467 (2023).
56. Reyer, C. P. O. *et al.* A plant's perspective of extremes: Terrestrial plant responses to changing climatic variability. *Global Change Biology* **19**, 75–89 (2013).

57. Maclean, I. Microclimf: Fast above, below or within canopy gridded microclimate modelling with R. (2021).
58. MacLean, I. Microclimf: Fast modelling of microclimate across real landscapes in R. https://ecoevorxiv.org/repository/view/9159/ (2025) doi:10.32942/x2bd17.
59. Lembrechts, J. J. *et al.* SoilTemp: A global database of near-surface temperature. *Global Change Biology* **26**, 6616–6629 (2020).
60. Maclean, I. M. D., Mosedale, J. R. & Bennie, J. J. Microclima: An R package for modelling meso- and microclimate. *Methods Ecol Evol* **10**, 280–290 (2019).
61. Karger, D. N. *et al.* Climatologies at high resolution for the earth's land surface areas. *Sci Data* **4**, 170122 (2017).
62. Karger, D. N. *et al.* Data from: Climatologies at high resolution for the earth's land surface areas. *EnviDat* (2021) doi:https://www.doi.org/10.16904/envidat.228.v2.1.
63. De Frenne, P. *et al.* Ten practical guidelines for microclimate research in terrestrial ecosystems. *Methods in Ecology and Evolution* **16**, 269–294 (2025).
64. Maclean, I. M. D., Suggitt, A. J., Wilson, R. J., Duffy, J. P. & Bennie, J. J. Fine-scale climate change: Modelling spatial variation in biologically meaningful rates of warming. *Global Change Biology* **23**, 256–268 (2017).
65. Klinges, D. H. *et al.* Proximal microclimate: Moving beyond spatiotemporal resolution improves ecological predictions. *Global Ecology and Biogeography* **n/a**, e13884 (2024).
66. Copernicus Climate Change Service. *ERA5: Fifth Generation of ECMWF Atmospheric Reanalyses of the Global Climate*. https://cds.climate.copernicus.eu/cdsapp#!/home (2017).
67. Duffy, J. P. Mcera5: Tools to acquire and process ERA5 data for use in microclimate modelling. R package version 0.2.0. (2021).

68. Isenburg, M. LASTools - effecient LiDAR processing software. rapidlasso (2014).
69. Milodowski, D. T. *et al.* The impact of logging on vertical canopy structure across a gradient of tropical forest degradation intensity in Borneo. *J Appl Ecol* **58**, 1764–1775 (2021).
70. Moeys, J. Soiltexture: Functions for soil texture plot, classification and transformation. R package version 1.5.1. (2018).
71. Poggio, L. *et al.* SoilGrids 2.0: Producing soil information for the globe with quantified spatial uncertainty. *SOIL* **7**, 217–240 (2021).
72. Helmer, E. H. *et al.* Detailed maps of tropical forest types are within reach: Forest tree communities for Trinidad and Tobago mapped with multiseason Landsat and multiseason fine-resolution imagery. *Forest Ecology and Management* **279**, 147–166 (2012).
73. R Core Team. R: A language and environment for statistical computing. R Foundation for Statistical Computing (2021).
74. García Molinos, J., Schoeman, D. S., Brown, C. J. & Burrows, M. T. VoCC: An r package for calculating the velocity of climate change and related climatic metrics. *Methods in Ecology and Evolution* **10**, 2195–2202 (2019).

10. ACKNOWLEDGEMENTS

LGS was supported by the W. Thomas Smith Scholarship from Davidson College.

11. EXTENDED DATA TABLES

Extended Data Table. 1: Climate velocity for maximum and minimum temperatures calculated from free-air, land-surface, and within-canopy climate conditions and the correlation between the direction of climate velocity and the direction of higher elevation or denser vegetation. Rho_{veg} and rho_{elev} represent correlation coefficients from circular correlations and p_{veg} and p_{elev} represent corresponding p-values.

Variable	Proximity	Resolution	Velocity (m/yr)	Temporal gradient (°C/yr)	Spatial gradient (m/yr)	rho_{veg}	p_{veg}	rho_{elev}	p_{elev}
Maximum temperature (°C)	Free-air	1km	76.145	0.025	<0.001	0.296	<0.001	0.921	<0.001
		100m	19.352	0.020	0.001	0.016	<0.001	0.957	<0.001
	Land-surface	1km	48.362	0.023	<0.001	0.438	<0.001	0.638	<0.001
		100m	9.821	0.023	0.002	0.366	<0.001	0.477	<0.001
		20m	3.442	0.024	0.007	0.141	<0.001	-0.289	<0.001
	Within-canopy	1km	0.472	0.027	0.057	0.138	<0.001	0.459	<0.001
		100m	0.372	0.027	0.072	0.112	<0.001	0.137	<0.001
		20m	0.280	0.027	0.096	-0.055	<0.001	-0.092	<0.001
Minimum temperature (°C)	Free-air	1km	27.950	0.010	<0.001	-0.106	<0.001	0.629	<0.001
		100m	9.485	0.009	0.001	0.017	<0.001	0.948	<0.001
	Land-surface	1km	10.127	0.002	<0.001	0.042	0.22	-0.538	<0.001

Variable	Proximity	Resolution	Velocity (m/yr)	Temporal gradient (°C/yr)	Spatial gradient (m/yr)	rho_{veg}	p_{veg}	rho_{elev}	p_{elev}
	Within-canopy	100m	1.267	0.002	0.002	-0.123	<0.001	0.379	<0.001
		20m	0.339	0.002	0.005	-0.238	<0.001	0.004	<0.001
		1km	0.446	0.004	0.009	-0.277	<0.001	0.112	<0.001
		100m	0.425	0.004	0.01	-0.086	<0.001	-0.445	<0.001
		20m	0.329	0.004	0.012	-0.023	<0.001	-0.072	<0.001

637

12. EXTENDED DATA FIGURES

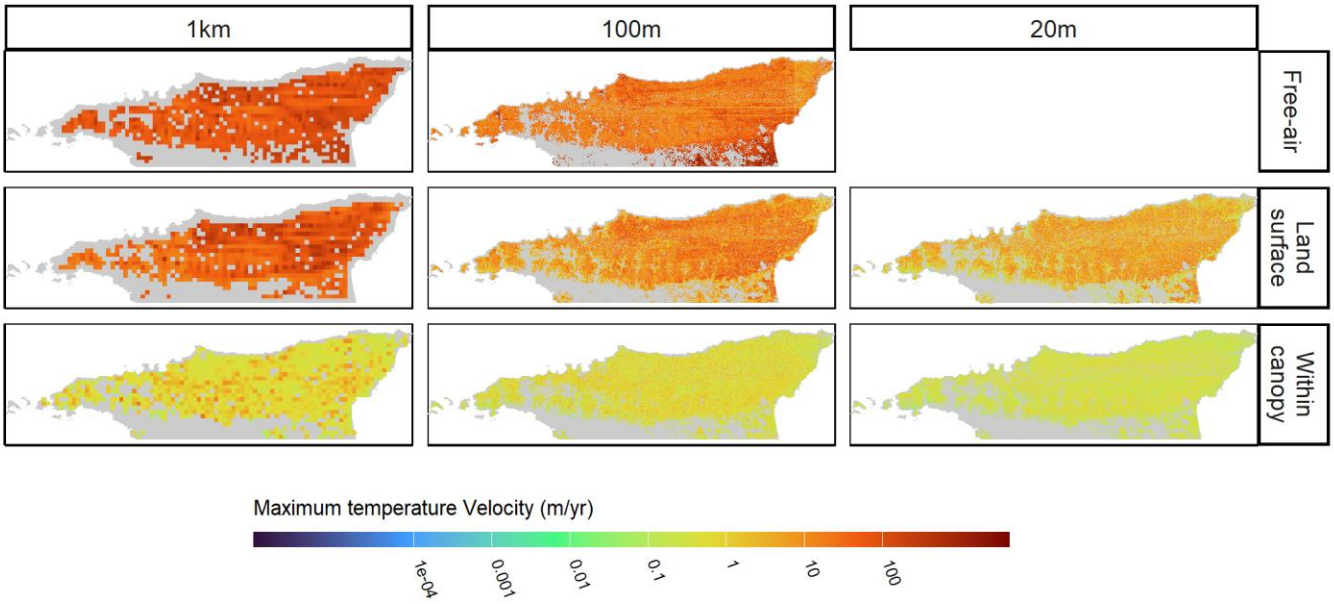

Extended Data Fig. 1: Maps of maximum temperature velocity in the Northern Range of Trinidad at different spatial scales for free-air, land surface, within-canopy conditions. Within canopy velocities represent the average velocity in the top half of the canopy.

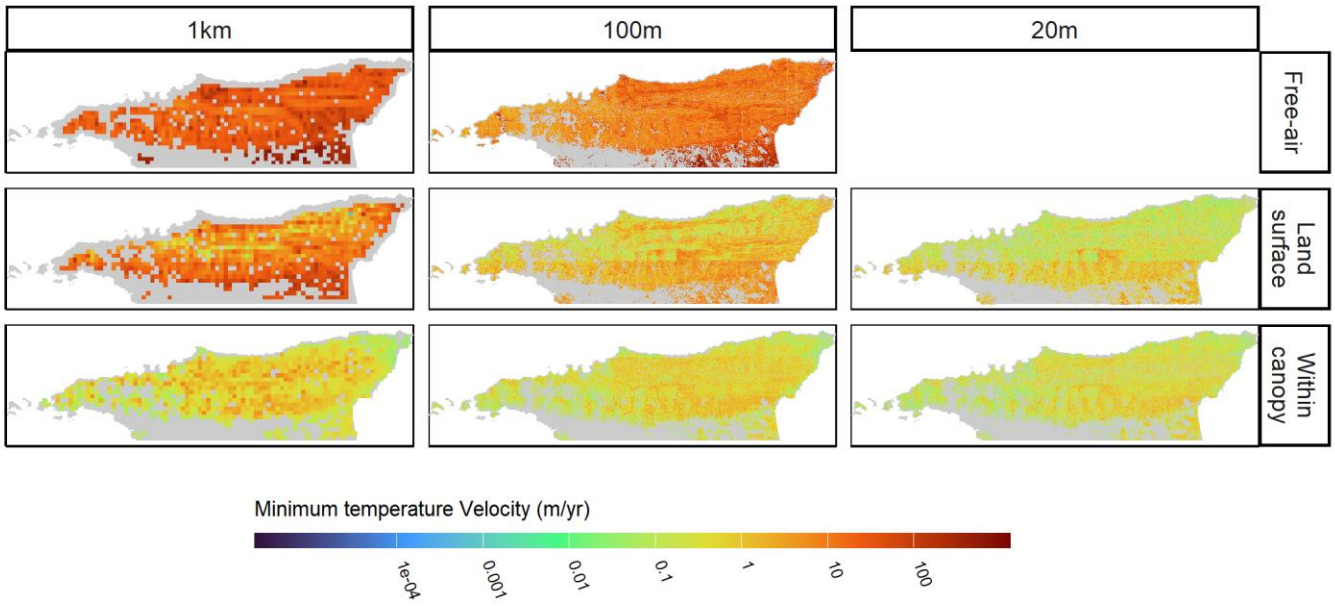

643

644 **Extended Data Fig. 2:** Maps of minimum temperature velocity in the Northern Range of

645 Trinidad at different spatial scales for free-air, land surface, and within-canopy conditions. Within

646 canopy velocities represent the average velocity in the top half of the canopy.

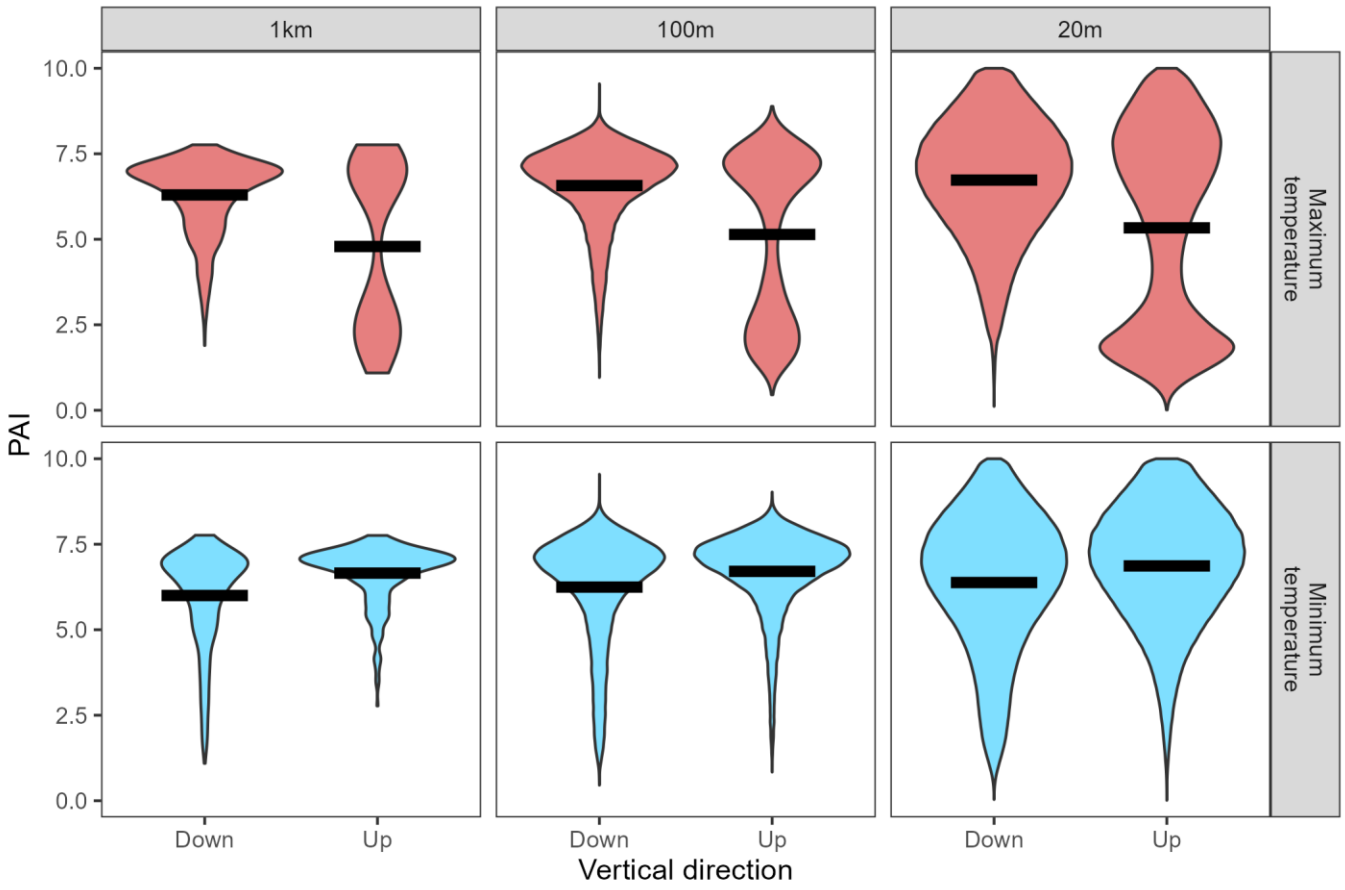

Extended Data Fig. 3: Distribution of plant area index (PAI) of upward and downward directed 3D velocity vectors at 1 km, 100 m, and 20 m spatial resolutions for maximum and minimum temperatures. Lines indicate means. PAI of downward directed maximum temperature velocities was consistently higher than upward directed velocities across spatial grains (1 km: $t_{175.43} = -8.17$, $p < 0.001$, 100 m: $t_{22390} = -86.05$, $p < 0.001$, 20 m: $t_{363815} = -287.17$, $p < 0.001$). PAI of downward directed minimum temperature velocities was lower than upward directed velocities across spatial grains (1 km: $t_{1038.9} = 11.36$, $p < 0.001$, 100 m: $t_{147917} = 69.35$, $p < 0.001$, 20 m: $t_{4305019} = 274.61$, $p < 0.001$)

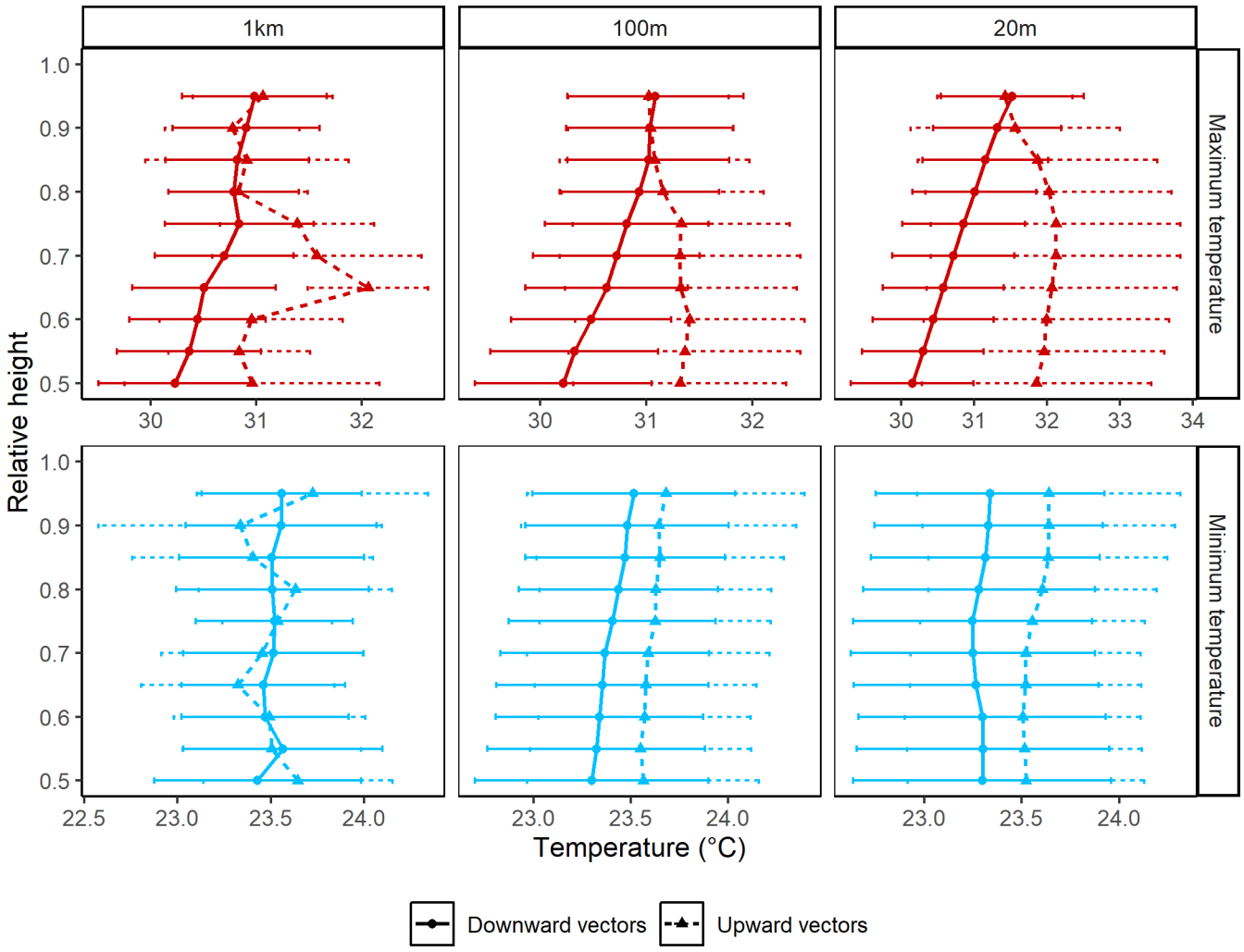

656

657 **Extended Data Fig. 4:** Vertical gradients (mean ± SD) for minimum and maximum temperatures
658 in the Northern Range of Trinidad at different spatial resolutions. Relative height indicates the
659 absolute height divided by the height of the canopy. Solid lines represent temperature mean and
660 SD of velocity vectors directed downward and dashed lines represent temperature mean and SD
661 of velocity vectors directed upward.

Supplementary material

S1 Plant area density maps

Plant area index (PAI) and plant area density (PAD) were estimated at a 1 m vertical resolution using a variant of the MacArthur-Horn method based on the Beer-Lambert law for light transmittance through a turbid medium[1,2]. The MacArthur-Horn method calculates PAD of voxels (i.e., spatial cubes) as the natural log of the ratio of pulses entering to pulses exiting a voxel of canopy space divided by the product of voxel height and the extinction coefficient. Milodowski et al.[2] modify the basic method to accommodate for the fact that each laser pulse gives rise to several returns. They weight points by the number of returns per pulse (Eq. 1):

$$PAD = \frac{1}{\kappa \Delta z} ln\left(\frac{\sum_{z=0}^{z=z_{i-1}} w_i}{\sum_{z=0}^{z=z_i} w_i}\right) \quad \text{Eq. 1}$$

Where K is the extinction coefficient, Δz is the voxel height, and $\underline{w_i}$ represents the points weighted by the number of returns associated with their respective LiDAR pulse. This approach assumes that the same area of foliage is intercepted by each return in a pulse[3] and therefore that pulses with more returns intercept less foliage at each return than pulses with fewer returns.

The extinction coefficient (K) is influenced by canopy characteristics, such as leaf angle, clumping, and reflectance. Field measurements are typically used to calibrate K, which varies with vegetation type but is well approximated by 0.5 for broadleaf tropical forests[4], as shown by comparisons of LAI estimates derived from airborne lidar scanning and field data[2,5,6].

We conducted a sensitivity analysis of PAI and PAD to determine the resolution at which microclimates would be modelled. PAI and PAD were estimated at 10 m, 20 m, 50 m, and 100 m resolutions. As resolution was coarsened, the variability of PAI and PAD within a 500 m x 500 m square extent decreased but finer details were lost. We chose to proceed modelling at a 20 m resolution, which eliminated extraneous outliers that appeared at a 10 m resolution while retaining the fine-scale variation in canopy structure that we wished to evaluate. We eliminated voxels below 2 m above the ground from PAI calculations as there were not consistently enough lidar returns in

understory layers to provide accurate estimations of vegetation density. At a 20 m resolution, ground returns and low-level returns were not present in several pixels. When this occurred, the resolution was iteratively expanded for the given height until lower level returns were present[2].

We estimated PAI and PAD seasonality based on leaf area index (LAI) derived from MODIS data. MODIS LAI corresponds well with ground-based LAI measurements in relatively open forests[7], and can therefore be used to predict PAI seasonality. Leaf area index for the Northern Range of Trinidad was downloaded from MCD15A3H Version 8 MODIS Level 4[8] at 4-day intervals from 1 January 2011 to 31 December 2020. LAI was averaged by day across 1000 randomly selected points within the study area. The 'mgcv' R package[9] was used to fit a generalised additive mixed model (GAMM) for mean LAI as a function of month. A first order auto-regressive moving-average (ARMA) correlation structure was used to account for temporal autocorrelation within each year. The order for the autoregression was determined by comparing first, second, and third order models with an ANOVA.

The seasonality pattern depicted in the MODIS LAI data was used to estimate PAI and PAD seasonality from the LiDAR based estimates. The offset between the MODIS-derived LAI and LiDAR-derived PAI and PAD were calculated in August for each grid cell. These offset values were then applied for each month of modelled LAI to estimate PAI and PAD seasonality at fine spatial scales. Note that we used August rather than June, which is when the LiDAR data were obtained, because the LiDAR data had a time stamp of August. We were only later informed that the LiDAR data were obtained in June. As both months occur during the wet season, the difference between MODIS and LiDAR measurements in June and August should be minimal.

S2 Macroclimate data from ERA5

ERA5 is an hourly climate dataset at a ~30 km resolution produced by the Copernicus Climate Change Service at ECMWF, and couples an atmospheric model with a land surface model to produce parameters such as temperature at 2 m above the ground that represent climate conditions in open fields. We obtained ERA5 data for two ten-year time periods: 1 January 1951 to 31 December 1960 (hereafter 'past') and 1 January 2011 to 31 December 2020 (hereafter 'present')[10]. Temperature at 2 m, dewpoint temperature at 2 m, surface pressure, the u and *v* components of mean windspeed (the east-west and north-south components), total precipitation,

total cloud cover, mean surface net longwave radiation flux, mean surface downward long wave radiation flux, total sky direct solar radiation at surface, and surface solar radiation were downloaded using the 'mcera5' R package[11]. Climatic variables, including temperature (°C), relative humidity (kPa), total incoming shortwave radiation (W/m^2), diffuse radiation (W/m^2), sky emissivity (0-1), windspeed (m/s), and wind direction (decimal degrees), were calculated for each ERA5 tile using the 'microctools' R package[12].

To increase computational efficiency, we selected one representative year from the past and present periods to use as input for the microclimate models. To select these years, we produced a generalised additive model of temperature at 2 m above the ground as a function of day of the year for each time period. The year for each time period with the lowest mean residuals was then selected to be used in the microclimate models. 1960 and 2015 were selected for past and present models, respectively. Climate change analyses therefore refer to changes that have occurred over a 55-year time period.

S3 Climate velocity

Temporal rate of climate change

For each climate variable (i.e., maximum temperature of the warmest month and minimum temperature of the coldest month), we calculated the temporal rate of change (°C/yr) for each grid cell, as the slope for the given climate variable between 1960 and 2015.

2D spatial rate of climate change

The spatial rate of climate change (°C/m) represents the average distance and direction in which climate is moving over the specified time interval. The 2D spatial rate is defined by vectors in the x (east-west) and y (north-south) directions. Each vector is calculated as the weighted average of pairwise differences between cells divided by the distance between the cell centres. We applied a weight of $1/\sqrt{2}$ to all pairwise differences that did not include the centre (focal) cell. This weight was chosen based trigonometric relationships in a 45-45-90 triangle. The x component of the spatial gradient for a given grid cell, *i*, is calculated as:

$$x_i = (\frac{c-w}{r_1} + \frac{e-c}{r_2} + \frac{n-nw}{r_3\sqrt{2}} + \frac{ne-n}{r_4\sqrt{2}} + \frac{s-sw}{r_5\sqrt{2}} + \frac{se-s}{r_6\sqrt{2}})/6$$

where *c* refers to the centre grid cell; *n*, *s*, *e*, and *w* refer to cells immediately north, south, east or west of the centre grid cell; *ne*, *nw*, *se*, and *sw* refer to cells sharing a corner with the centre grid cell; and r_i is the distance between the centres of the respective grid cells, which we adjusted based on simple trigonometric relationships to account for the impact of elevation on the distance between grid cells (Figure 1,2). This method is modified from Burrows et al.[13].

The y component of the spatial gradient is defined as:

$$y_i = (\frac{n-c}{r_1} + \frac{c-s}{r_2} + \frac{nw-w}{r_3\sqrt{2}} + \frac{w-sw}{r_4\sqrt{2}} + \frac{ne-e}{r_5\sqrt{2}} + \frac{e-se}{r_6\sqrt{2}})/6$$

We then calculated the spatial rate for each grid cell, *i*, as $magnitude_i = \sqrt{{x_i}^2 + {y_i}^2}$.

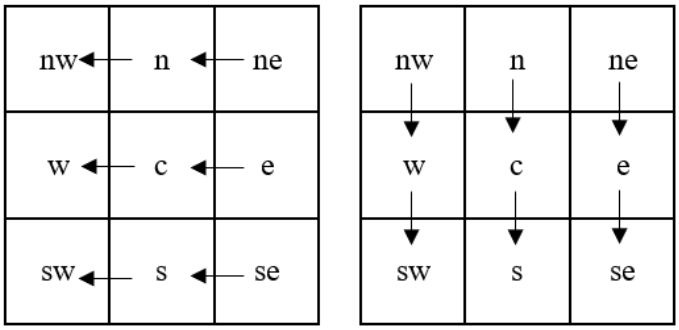

Figure 1. Components of the 2D spatial rate of climate change
Here, *c* refers to the centre (focal) cell.

3D spatial rate of climate change

The 3D spatial rate is defined by vectors in the x, y, and z (canopy to ground) dimensions. There are six components to the three-dimensional spatial rate, each defined by the climatic difference between the centre focal cell and an adjacent cell and the spatial distance between the centres of the two cells (Figure 3). The spatial rate in each dimension is then calculated as the mean between the two contributing rates. For example, the east-west gradient is:

$$(\frac{e - focal}{r_1} + \frac{focal - w}{r_2})/2$$

Distance in the vertical dimension was determined by the height difference between the focal cell and the cell above or below.

Note that the climate velocity at 5 m above the ground was calculated using a vertical resolution of 3 m below the focal layer and 5 m above the focal layer, because 2 m above the ground was the lowest microclimate layer modelled. Additionally, top and bottom climate layers (2 m and 40 m above the ground) were excluded because there was no layer below or above, respectively, that could be used for the calculation. We adjusted the spatial distance based on simple trigonometric relationships to account for elevational change between cells using the same method as 2D velocities. From the three vectors, we calculated the spatial rate for each grid cell, i: $spatial\ rate_i = \sqrt{{x_i}^2 + {y_i}^2 + {z_i}^2}$.

The 3D methods differ slightly from the 2D methods and those described in Burrows et al.[13] because they only include cells adjacent to the focal cell and do not include cells that touch at a corner. We chose to only include adjacent cells in calculations of 3D velocity because they have the most direct effect on the spatial rate of the focal cell and comply more intuitively with a 3D framework.

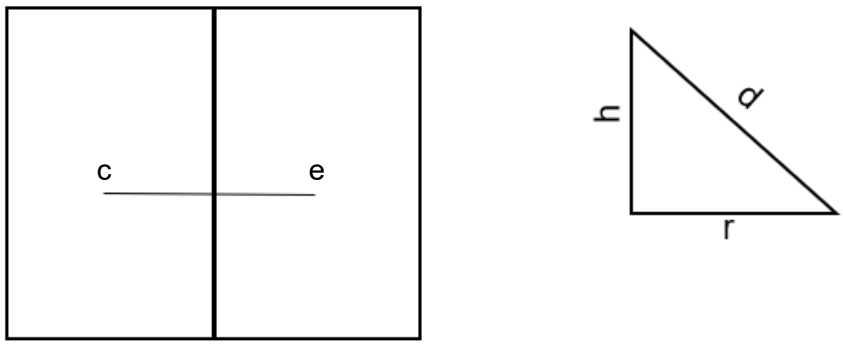

Figure 2. Elevation correction for the distance between cells
The climatic difference is calculated as e - c. The triangle represents the elevational adjustment. The resolution (*r*) is the distance between cell centres that would be observed from above, and *h*

is the elevational gain moving from the east cell to the focal cell. Therefore, the distance required to move from b to a is $d = \sqrt{h^2 + r^2}$. The spatial rate, *s,* between these two cells is then calculated as $s = (e - c)/\sqrt{h^2 + r^2}$. This method is modified from Burrows et al. [13].

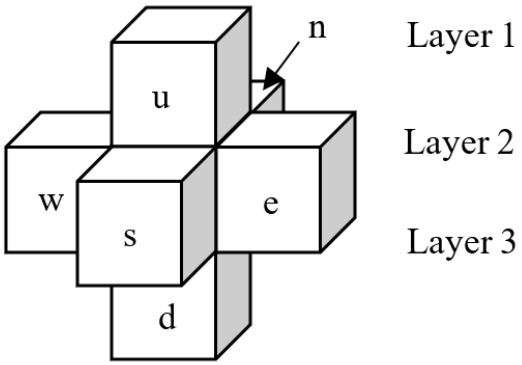

Figure 3. Voxels to calculate the spatial rate of 3D microclimate velocity.

Velocity

Climate velocity is calculated by dividing the temporal rate by the spatial rate. Positive values indicate the climate is warming and negative values indicate the climate is cooling. The direction of climate velocity is based on the direction of the spatial and temporal rates. For example, if temperature only changes in the east-west direction, if the climate is warming over time (positive temporal rate) and temperature increases from west to east (positive spatial rate), the direction of climate velocity should point due west. In contrast if the climate is cooling over time (negative temporal rate) and the temperature still increases from west to east, the direction of climate velocity should point due east. We therefore multiplied the vectors describing the spatial gradient by -1 if the temporal gradient was positive, so that the directional vectors always point toward cooler climates when the climate is warming over time and warmer climates when the climate is cooling over time. Using these adjusted vectors, we calculated the direction of climate movement in the latitude/longitude plane as the angle from north and in the vertical dimension for 3D vectors as angle from horizontal, where horizontal is in reference to the ground. (Horizontal can therefore refer to non-horizontal movement if on a slope.) The vertical-dimension angle ranges from -90° to

90°, where -90° indicates movement directly downward with no horizontal movement and 90° indicates movement directly upward with no horizontal movement.

References

1. MacArthur, R. H. & Horn, H. S. Foliage profile by vertical measurements. *Ecology* **50**, 802–804 (1969).
2. Milodowski, D. T. *et al.* The impact of logging on vertical canopy structure across a gradient of tropical forest degradation intensity in Borneo. *J Appl Ecol* **58**, 1764–1775 (2021).
3. Armston, J. *et al.* Direct retrieval of canopy gap probability using airborne waveform lidar. *Remote Sensing of Environment* **134**, 24–38 (2013).
4. Martens, S. N., Ustin, S. L. & Rousseau, R. A. Estimation of tree canopy leaf area index by gap fraction analysis. *Forest Ecology and Management* **61**, 91–108 (1993).
5. Tang, H. *et al.* Retrieval of vertical LAI profiles over tropical rain forests using waveform lidar at La Selva, Costa Rica. *Remote Sensing of Environment* **124**, 242–250 (2012).
6. Tang, H. *et al.* Deriving and validating Leaf Area Index (LAI) at multiple spatial scales through lidar remote sensing: A case study in Sierra National Forest, CA. *Remote Sensing of Environment* **143**, 131–141 (2014).
7. Clark, D. B., Olivas, P. C., Oberbauer, S. F., Clark, D. A. & Ryan, M. G. First direct landscape-scale measurement of tropical rain forest Leaf Area Index, a key driver of global primary productivity. *Ecology Letters* **11**, 163–172 (2008).
8. Myneni, R., Knyazikhin, Y. & Park, T. MCD15A3H MODIS/Terra+Aqua leaf area index/FPAR 4-day L4 global 500m SIN grid V006. (2015).
9. Wood, S. *Generalized Additive Models: An Introduction with R (2nd Edition)*. (Chapman and Hall/CRC, 2017).

10. Copernicus Climate Change Service (C3S). *ERA5: Fifth Generation of ECMWF Atmospheric Reanalyses of the Global Climate*. https://cds.climate.copernicus.eu/cdsapp#!/home (2017).
11. Duffy, J. P. mcera5: Tools to acquire and process ERA5 data for use in microclimate modelling. R package version 0.2.0. (2021).
12. Maclean, I. microctools: Various worker functions for microclimc package. R package version 0.1.0. (2021).
13. Burrows, M. T. *et al.* The pace of shifting climate in marine and terrestrial ecosystems. *Science* **334**, 652–655 (2011).

S4 Supplementary tables and figures

Table S 1: Median 2D climate velocities (m/yr), temporal gradients (°C/yr), and spatial gradients (°C/m) for maximum and minimum temperatures in the top quarter of the canopy (canopy) and at 2 m above the ground (land surface).

Resolution	Variable	Height	Velocity (m/yr)	Temporal gradient (°C/yr)	Spatial gradient (°C/m)
100m	Maximum temperature	Canopy	19.362	0.028	0.001
		Land surface	9.818	0.023	0.002
	Minimum temperature	Canopy	4.114	0.004	0.001
		Land surface	1.239	0.002	0.002
1km	Maximum temperature	Canopy	99.422	0.027	<0.001
		Land surface	43.695	0.023	<0.001
	Minimum temperature	Canopy	20.134	0.004	<0.001
		Land surface	9.827	0.002	<0.001
20m	Maximum temperature	Canopy	3.114	0.028	0.009

Resolution	Variable	Height	Velocity (m/yr)	Temporal gradient (°C/yr)	Spatial gradient (°C/m)
		Land surface	4.259	0.023	0.005
	Minimum temperature	Canopy	1.251	0.005	0.004
		Land surface	0.331	0.002	0.005

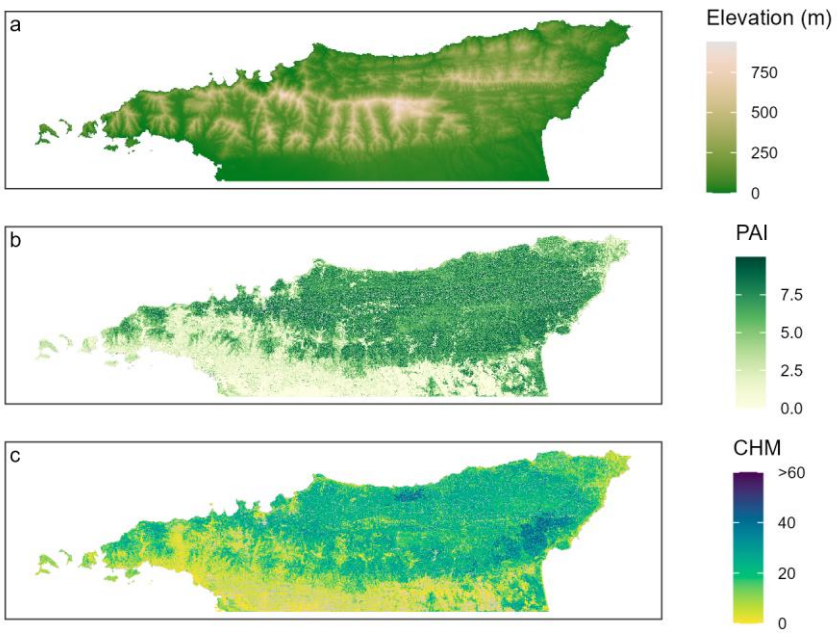

Fig. S1: Elevation (m), plant area index (PAI), and the canopy height model (CHM) for the northern mountain range of Trinidad. Maps were derived from a LiDAR survey of the northern range conducted in June 2014.

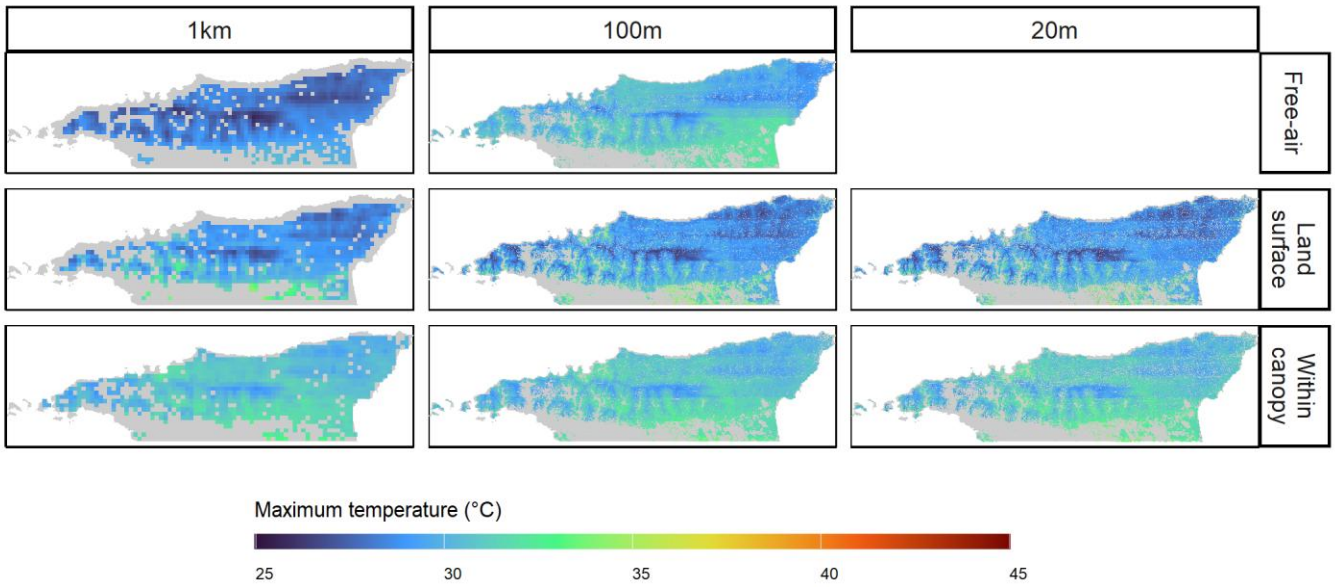

Fig. S2: Maximum temperatures for free-air conditions at 1 km and 100 m resolutions, land surface temperatures at 2 m above the ground and at 1 km, 100 m, and 20 m resolutions, and within-canopy temperatures in the upper half of the canopy (as measured from the ground to the top of the canopy) at 1 km, 100 m, and 20 m spatial resolutions.

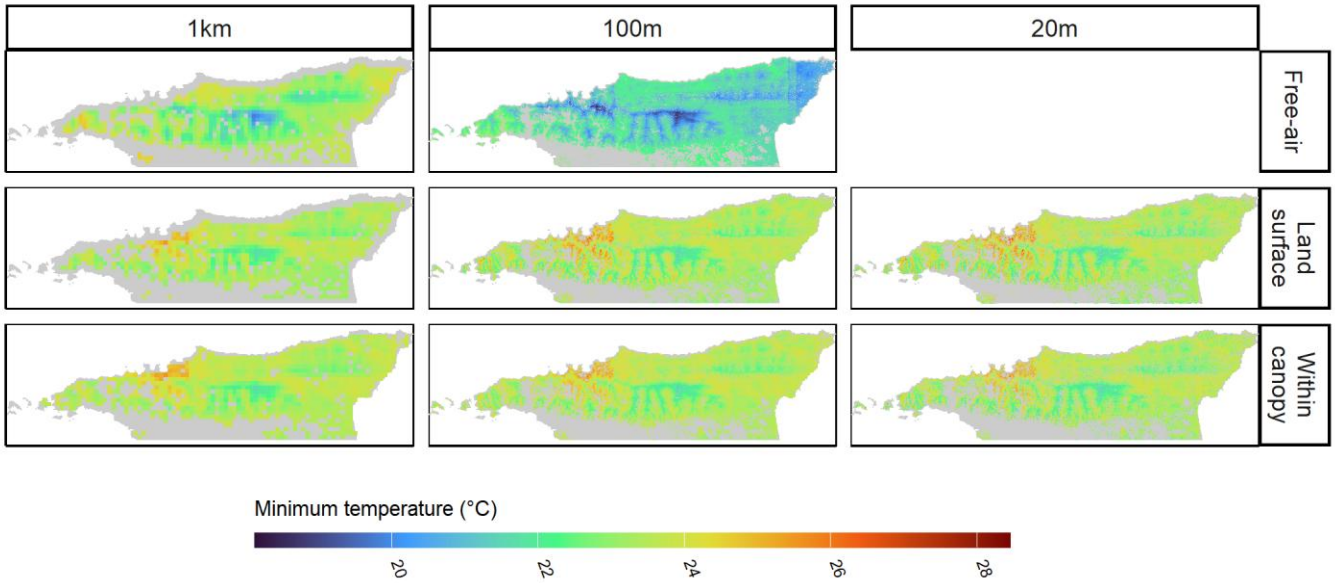

Fig. S3: Minimum temperatures for free-air conditions at 1 km and 100 m resolutions, land surface temperatures at 2 m above the ground and at 1 km, 100 m, and 20 m resolutions, and within-canopy temperatures in the upper half of the canopy (as measured from the ground to the top of the canopy) at 1 km, 100 m, and 20 m spatial resolutions.

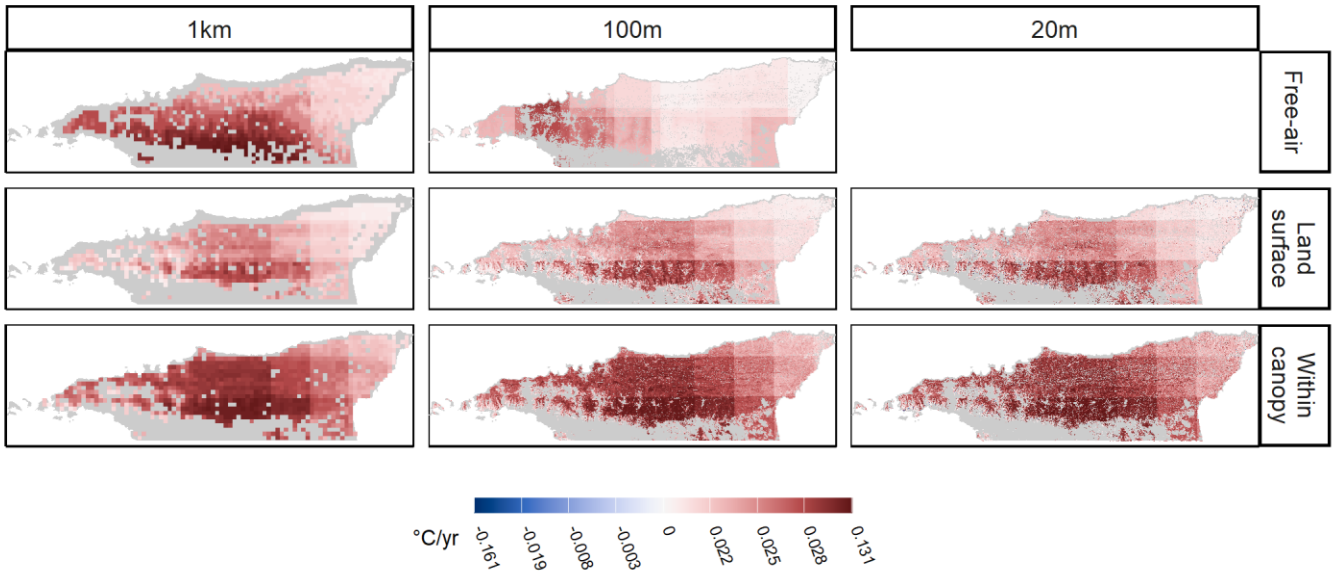

Fig. S4: Temporal gradient of maximum temperature velocity for free-air temperatures, land surface temperatures at 2 m above the ground, and within-canopy temperatures at 1 km, 100 m, and 20 m spatial resolutions.

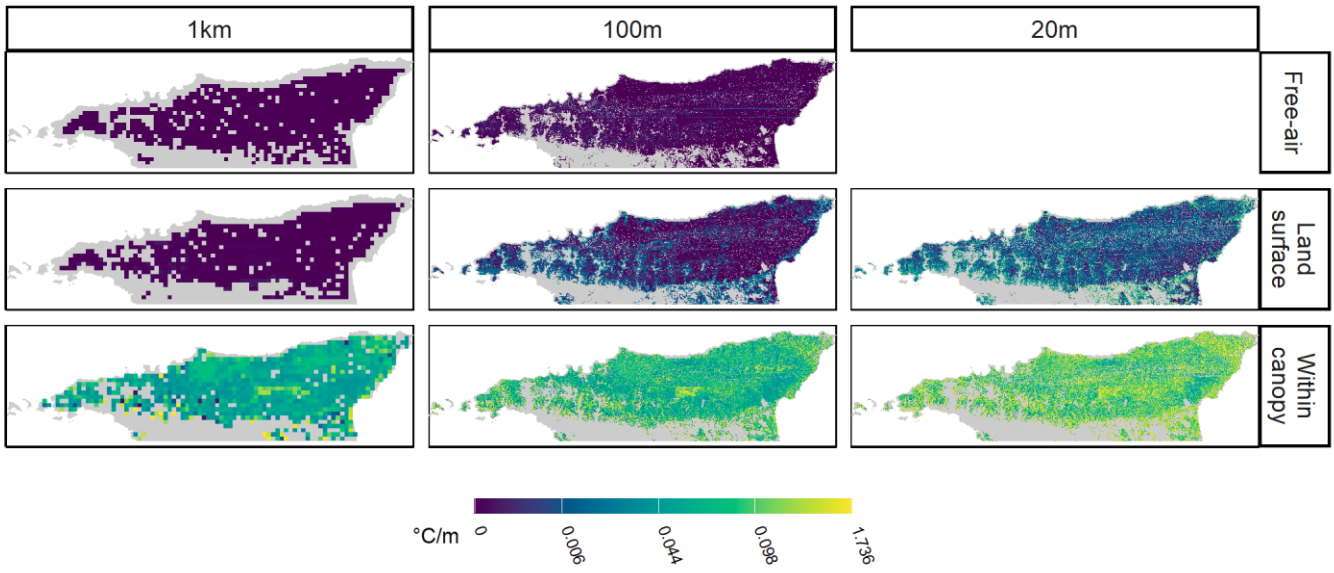

Fig. S5: Spatial gradient of maximum temperature velocity for free-air temperatures, land surface temperatures at 2 m above the ground, and within-canopy temperatures at 1 km, 100 m, and 20 m spatial resolutions.

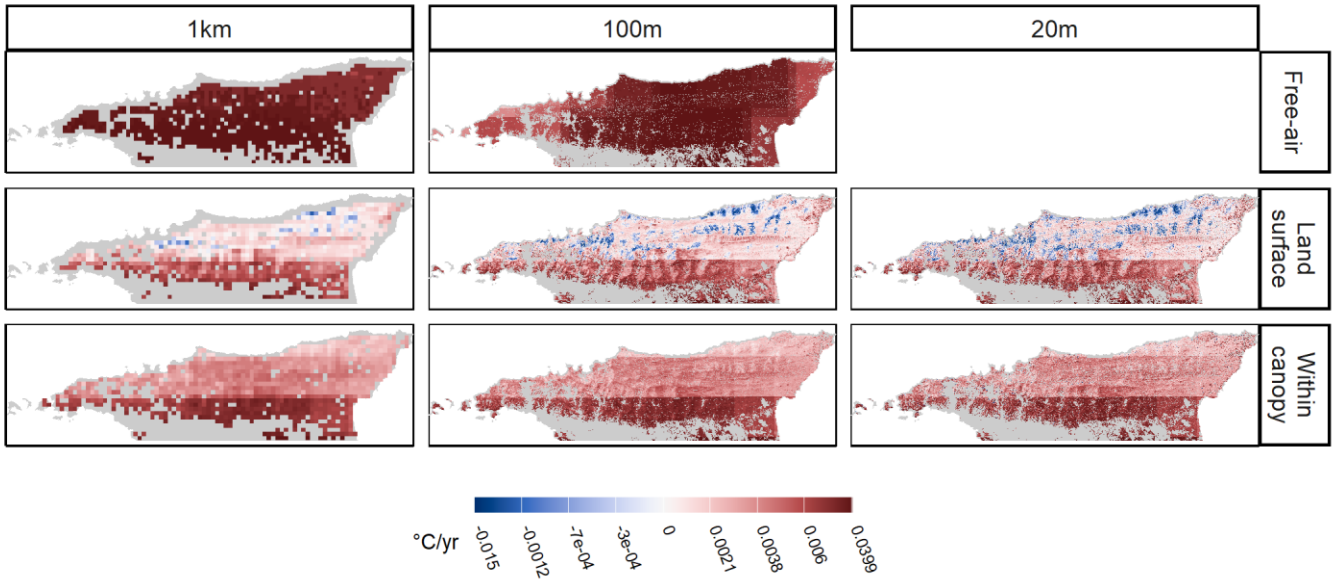

Fig. S6: Temporal gradient of minimum temperature velocity for free-air temperatures, land surface temperatures at 2 m above the ground, and within-canopy temperatures at 1 km, 100 m, and 20 m spatial resolutions.

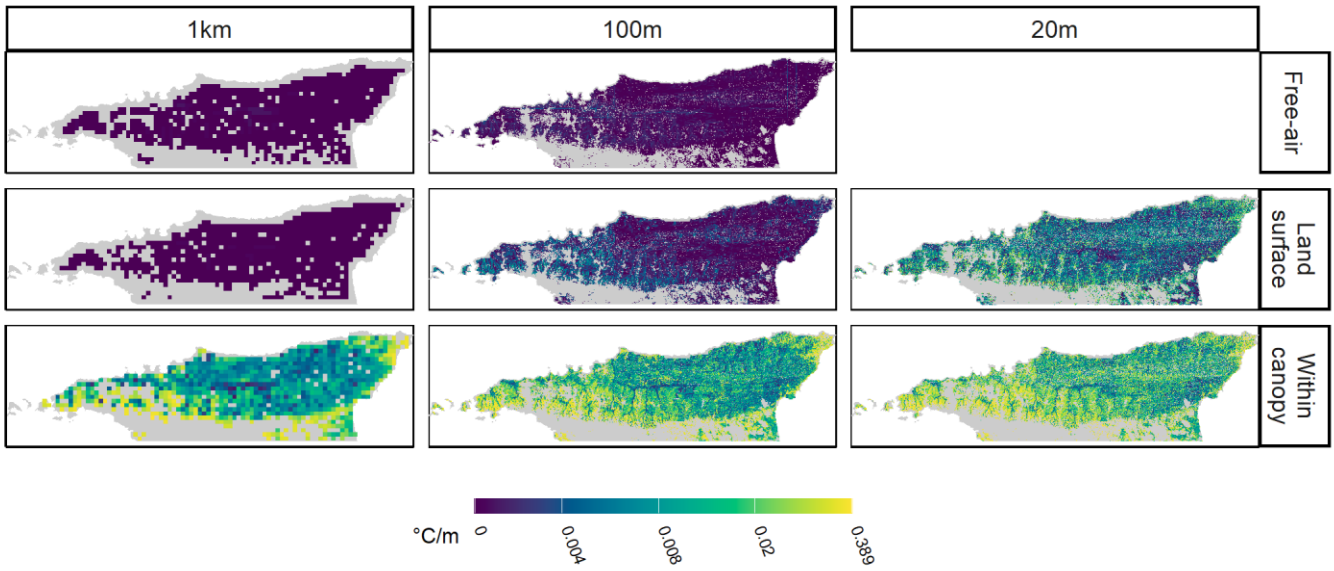

Fig. S7: Spatial gradient of minimum temperature velocity for free-air temperatures, land surface temperatures at 2 m above the ground, and within-canopy temperatures at 1 km, 100 m, and 20 m spatial resolutions.

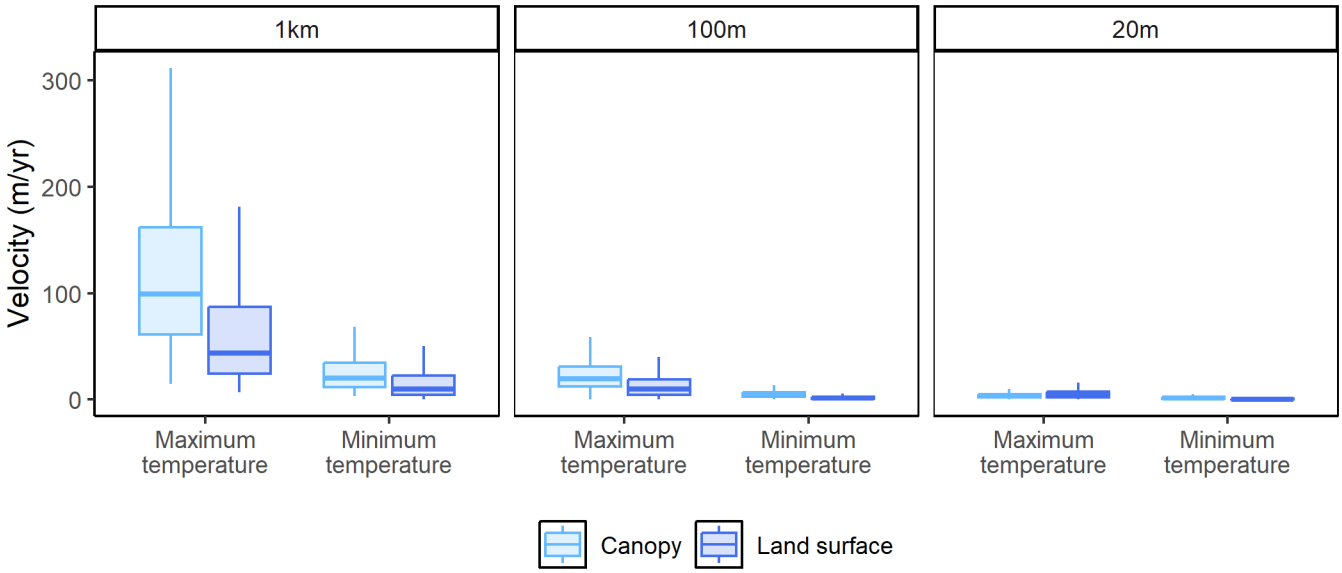

Fig. S8: 2D climate velocities for maximum and minimum temperatures in the top quarter of the canopy (canopy) and 2 m above the ground (land surface) at 1 km, 100 m, and 20 m spatial scales in the Northern Range of Trinidad.